

On Variance Reduction in Learning Mean Flows

Juanwu Lu
Purdue University
juanwu@purdue.edu

Ziran Wang
Purdue University
ziran@purdue.edu

Abstract

One-step generative modeling has emerged as a leading approach to amortize the inference cost of diffusion and flow-matching models. Among distillation-free methods, MeanFlow training is notoriously unstable, with non-decreasing loss and unbounded gradient variance. In this work, we establish a theory that attributes this pathology to a misuse of the conditional velocity field: it plays two distinct statistical roles in the loss, both as an unbiased regression target and as a Monte Carlo control variate inside a Jacobi-vector product, with the original loss assigning the wrong coefficient to the latter. We derive the optimal coefficient in closed form, and show that a family of fixes in concurrent works corresponds to different practical realizations of the same optimum. A controlled sweep of this coefficient on two-dimensional benchmarks and on a latent Diffusion Transformer recovers the predicted bias-variance ordering. The optimal coefficient yields up to a 54% improvement in sample quality on two-dimensional benchmarks and a monotone FID trend at every matched-step DiT checkpoint. Crucially, the same DiT measurement also reveals a quantitative *FID-MSE landscape mismatch*: although gradient variance is minimized at an interior coefficient value, the coefficient that minimizes FID prefers the direct use of conditional velocity.

Keywords One-step Generative Models, Mean Flows, Variance Reduction, Control Variate

1 Introduction

Deep generative models that leverage neural networks to parametrize and sample from unknown data distributions have achieved remarkable success [1–5]. Among these models, flow-based generative models [6–12] learn a continuous-time transformation between a simple prior and the data distribution. Conditional flow matching [10, 11] and stochastic interpolants [12, 13] further enable simulation-free training by regressing a velocity field, achieving sample quality competitive with diffusion models [1, 14, 2]. However, integration at inference time remains a challenge due to its computational costs and numerical instability, motivating a series of subsequent works on *one-step generative models*, including progressive distillation [15], distribution matching [16, 17], consistency models [18, 19], and flow map matching [20]. Nevertheless, most of them require a pre-trained distillation teacher.

Mean Flows [21] provide a *distillation-free* alternative by learning a two-parameter average velocity field through least-squares regression of a total-derivative identity between the average and instantaneous velocity. In principle, this identity yields exact self-supervision. In practice, however, training is plagued by *non-decreasing loss* and prohibitively *high gradient variance* [22, 23]. A plethora of concurrent works have proposed remedies that target different mechanisms. AlphaFlow [22] attributes slow convergence to gradient conflict between flow-matching and total-derivative consistency components and proposes an α -curriculum. Improved MeanFlow [23] replaces the conditional-velocity tangent with a learned marginal-velocity head. Re-MeanFlow [24] preprocesses the data with rectified-flow straightening to reduce trajectory curvature. Terminal Velocity Matching [25] sidesteps the spatial Jacobian by differentiating with respect to the terminal time. Functional Mean Flows [26] extend MeanFlow to Hilbert spaces and study marginal-conditional consistency for functional data. Each fix is empirically effective in isolation, but no theory explains *why* the original objective is unstable or *what* these fixes have in common.

arXiv:2605.09235v1 [cs.LG] 10 May 2026

In this paper, we establish our theory around a single research question:

Why do stochastic tangents destabilize learning Mean Flows?

We answer this question through the lens of *variance reduction*. Specifically, we identify that the conditional velocity plays two statistically distinct roles in the MeanFlow loss. As the regression target, it is an *unbiased* estimator of the marginal velocity. As the tangent inside the Jacobian-vector product (JVP) of the total-derivative identity, however, it acts as a Monte Carlo *control variate* for the inaccessible marginal velocity, with a statistically suboptimal coefficient. The bias-variance trade-off induced by this substitution governs the variance of the gradient through a quadratic term. A Jacobi factor in JVP amplifies sample-based conditional fluctuations at each gradient step, and stop-gradient further hides this amplification from the optimizer, leading to the empirical pathology.

Following the theory, we derive the optimal tangent control-variate coefficient in closed form and show that it converges to a deterministic-tangent estimator in the practical regime where a marginal-velocity estimator is available. This result *explains* why deterministic tangents (*e.g.*, *learned velocity heads*) help stabilize training. They are essentially different practical instantiations of the same statistical optimum. To empirically validate the framework, we perform a controlled sweep of the coefficient across two-dimensional datasets and the ImageNet dataset using latent diffusion Transformers (DiTs). Direct measurement of per-step gradient variance recovers the predicted non-decreasing loss component. Meanwhile, we observe a $1.2\times \sim 4.3\times$ reduction with deterministic tangents on the two-dimensional datasets. The same sweep on ImageNet also reveals a quantitative *FID-MSE landscape mismatch*: the FID ordering aligns with the bias-variance prediction across all four coefficient values. Nonetheless, the FID-axis offset ratio across large coefficients is super-linear in the MSE-axis, hence the FID-optimal coefficient shifts past the gradient-MSE interior minimizer to the *unbiased* corner. Our contributions in this paper are as follows:

- C1** We establish a theory to prove that per-step gradient variance in the original MeanFlow scales unboundedly with the spatial-Jacobi factor in JVP and the stop-gradient operator induces a *semi-gradient gap* that hides this term from the optimizer.
- C2** We frame the JVP tangent as a *control variate* for the marginal velocity, derive the optimal coefficient in closed form, and unify concurrent works by showing that they each correspond to a different practical realization of the optimal coefficient.
- C3** We empirically validate the framework through a controlled sweep of the coefficient on both two-dimensional datasets and ImageNet with latent DiTs. We observe $1.2\times \sim 4.3\times$ direct gradient-variance reduction, up to 54% SW_1 improvements on two-dimensional benchmarks, the predicted bias-variance FID ordering at every matched-step DiT checkpoint, and a quantitative FID-MSE landscape mismatch: the optimal coefficient minimizing gradient-MSE is near 0.94. In contrast, the one that minimizes FID leans toward 0.

2 Preliminaries

Flow-Matching. Let \mathbf{x} denote a data sample in $\mathcal{X} \subset \mathbb{R}^d$. Flow-matching generative models [10, 11] learn a time-dependent diffeomorphism $\psi(\mathbf{x}, t) : \mathbb{R}^d \times [0, 1] \rightarrow \mathbb{R}^d$ from a simple distribution $\mathbf{x}_1 \sim p(\mathbf{x}, 1)$ to the target $\mathbf{x}_0 \sim p(\mathbf{x}, 0) = p_{\text{data}}$ by parameterizing a velocity field $\mathbf{v}(\mathbf{x}, t) \triangleq \frac{d}{dt}\psi(\mathbf{x}, t)$. Since the exact *marginal velocity field* $\mathbf{v}(\mathbf{x}, t)$ is generally inaccessible, conditional flow-matching [10] instead learns a conditional field $\mathbf{v}_{\text{cond}} = \mathbf{x}_1 - \mathbf{x}_0$ with $\mathbf{x}_t = (1-t)\mathbf{x}_0 + t\mathbf{x}_1$. The following lemma justifies the substitution. See Appendix B.1 for its proof.

Lemma 1. *Given vector fields \mathbf{v}_{cond} generating conditional probability paths $p(\mathbf{x}, t | \mathbf{x}_0)$, for any $\mathbf{x}_0 \sim p(\mathbf{x}_0)$, the expected conditional velocity field is equal to the marginal velocity field*

$$\mathbf{v}(\mathbf{x}, t) = \mathbb{E}_{\mathbf{x}_0 \sim p(\mathbf{x}_0 | \mathbf{x}_t = \mathbf{x})}[\mathbf{v}(\mathbf{x}, t | \mathbf{x}_0)]. \tag{1}$$

One-step Mean Flows. Iterative integration of $\mathbf{v}(\mathbf{x}, t)$ at inference is expensive and can be numerically unstable. To bypass it, Mean Flows [21] learn a two-parameter average velocity field $\mathbf{u}(\mathbf{x}, r, t)$ through regressing an identity along the flow trajectory $\mathbf{x}_\tau = \psi(\mathbf{x}_r, \tau)$ with terminal at $\mathbf{x}_t = \mathbf{x}$:

$$(t - r) \mathbf{u}(\mathbf{x}, r, t) = \int_r^t \mathbf{v}(\mathbf{x}_\tau, \tau) d\tau. \tag{2}$$

Differentiating with respect to the terminal time t along the same trajectory yields

$$\mathbf{u}(\mathbf{x}, r, t) + (t - r) \frac{d}{dt} \mathbf{u}(\mathbf{x}, r, t) = \mathbf{v}(\mathbf{x}, t), \quad \frac{d}{dt} \mathbf{u} = \partial_{\mathbf{x}} \mathbf{u} \cdot \mathbf{v}(\mathbf{x}, t) + \partial_t \mathbf{u}, \quad (3)$$

where the total derivative $\frac{d}{dt} \mathbf{u}$ is essentially a JVP, denoted by $\text{JVP}(\mathbf{u}, (\mathbf{x}, r, t), (\mathbf{v}(\mathbf{x}, t), 0, 1))$. The original MeanFlow paper [21] replaces *both* occurrences of the marginal field with the conditional field $\mathbf{v}_{\text{cond}} = \mathbf{x}_1 - \mathbf{x}_0$, giving the MeanFlow loss

$$\mathcal{L}_{\text{MF}}(\boldsymbol{\theta}) = \mathbb{E}_{r, t, \mathbf{x}_0, \mathbf{x}_1} \left[\left\| \mathbf{u}_{\boldsymbol{\theta}} + (t - r) \text{sg}[\text{JVP}(\mathbf{u}_{\boldsymbol{\theta}}, (\mathbf{x}_t, r, t), (\mathbf{v}_{\text{cond}}, 0, 1))] - \mathbf{v}_{\text{cond}} \right\|_2^2 \right], \quad (4)$$

with $r, t \sim \mathcal{U}(0, 1)$, $r \leq t$, $\mathbf{x}_0 \sim p_{\text{data}}$, $\mathbf{x}_1 \sim \mathcal{N}(0, \mathbf{I}_d)$, $\mathbf{x}_t = (1 - t)\mathbf{x}_0 + t\mathbf{x}_1$, and the stop-gradient $\text{sg}[\cdot]$ avoiding double backpropagation through the JVP.

3 Variance Reduction in Learning Mean Flows

The MeanFlow loss in equation 4 is empirically known to be *non-decreasing* and to suffer from *high-variance gradients* [22, 23]. We investigate the statistical mechanism behind this pathology. Importantly, our analysis isolates the role of the conditional velocity field \mathbf{v}_{cond} when it appears as the JVP tangent, and identifies that it acts as a Monte Carlo control variate for the inaccessible marginal velocity, with a coefficient that the original MeanFlow fixes to a suboptimal value. We derive the optimal coefficient and establish a connection to practical fixes in concurrent works.

3.1 Two roles of the conditional velocity field

With Reynolds decomposition, we express the conditional velocity by $\mathbf{v}_{\text{cond}} = \mathbf{v}(\mathbf{x}, t) + \mathbf{v}'$ with $\mathbb{E}_{\mathbf{x}_0 | \mathbf{x}_t}[\mathbf{v}'] = \mathbf{0}$ according to equation 1 and $\Sigma_{\mathbf{v}'} \triangleq \text{Cov}_{\mathbf{x}_0 | \mathbf{x}_t}[\mathbf{v}']$. The MeanFlow loss in equation 4 uses \mathbf{v}_{cond} both as the *regression target* and as the *tangent* inside the total derivative. Carrying the decomposition through per-sample loss $\ell_{\text{MF}}(\boldsymbol{\theta})$ yields:

$$\mathbb{E}_{\mathbf{x}_0 | \mathbf{x}_t}[\ell_{\text{MF}}(\boldsymbol{\theta})] = \left\| \mathbf{r}_{\boldsymbol{\theta}}^{\text{sg}} \right\|_2^2 + \text{sg}[\text{Tr}(\mathbf{J} \Sigma_{\mathbf{v}'} \mathbf{J}^{\top})], \quad (5)$$

where $\mathbf{J} \triangleq (t - r) \partial_{\mathbf{x}_t} \mathbf{u}_{\boldsymbol{\theta}} - \mathbf{I}_d \in \mathbb{R}^{d \times d}$ is a *Jacobi factor* determined by the Jacobian matrix $\partial_{\mathbf{x}_t} \mathbf{u}_{\boldsymbol{\theta}}$ and $\mathbf{r}_{\boldsymbol{\theta}}^{\text{sg}} \triangleq \mathbf{u}_{\boldsymbol{\theta}} + (t - r) \text{sg}[\partial_{\mathbf{x}_t} \mathbf{u}_{\boldsymbol{\theta}} \cdot \mathbf{v} + \partial_t \mathbf{u}_{\boldsymbol{\theta}}] - \mathbf{v}$ is the deterministic mean-field residual. Since the residual $\mathbf{r}_{\boldsymbol{\theta}}^{\text{sg}}$ is the exact loss we aim to minimize given by equation 3, the trace term leads to the non-decreasing loss and eliminates *iff* the Jacobi satisfies $\partial_{\mathbf{x}_t} \mathbf{u}_{\boldsymbol{\theta}} = \frac{1}{t - r} \mathbf{I}_d$ (equivalently, $\mathbf{J} = \mathbf{0}$). We identify two roles of the conditional velocity field in this decomposition:

Unbiased Target. As the regression target, \mathbf{v}_{cond} injects \mathbf{v}' *linearly* into the residual, contributing the *irreducible* per-sample noise floor $\text{Tr}(\Sigma_{\mathbf{v}'})$. However, since this noise is independent of $\boldsymbol{\theta}$ and \mathbf{v}' is zero-mean, \mathbf{v}_{cond} can serve as an unbiased target for learning Mean Flows.

Variance Amplifier. As the JVP tangent, the same \mathbf{v}_{cond} injects \mathbf{v}' *multiplicatively* through the Jacobi factor \mathbf{J} , contributing the *amplified* term $\text{Tr}(\mathbf{J} \Sigma_{\mathbf{v}'} \mathbf{J}^{\top})$. It scales unboundedly with the spectral magnitude of \mathbf{J} . This amplification is the dominant driver of variance at the gradient level:

Theorem 2 (Jacobian Variance Amplification). *Let $\mathbf{g} \triangleq \nabla_{\boldsymbol{\theta}} \mathbf{u}_{\boldsymbol{\theta}}(\mathbf{x}_t, r, t) \in \mathbb{R}^{d \times p}$ be the parameter Jacobian of the average velocity. The trace of the conditional gradient covariance (i.e., the total variance) of $\ell_{\text{MF}}(\boldsymbol{\theta})$ in equation 4 satisfies*

$$\text{Tr}(\text{Cov}[\nabla_{\boldsymbol{\theta}} \ell_{\text{MF}} | \mathbf{x}_t]) \propto \text{Tr}(\mathbf{g}^{\top} \mathbf{J} \Sigma_{\mathbf{v}'} \mathbf{J}^{\top} \mathbf{g}). \quad (6)$$

See the proof in Appendix B. The theorem identifies that the total gradient variance grows with $\|\mathbf{J}\|^2$ for fixed \mathbf{g} and $\Sigma_{\mathbf{v}'}$, saturates only at the irreducible noise floor when $\mathbf{J} \rightarrow \mathbf{0}$, and is *uncontrolled* by any term in the loss due to the use of the stop-gradient in the original MeanFlow. Meanwhile, without the stop-gradient operator, the optimizer could in principle reduce variance by driving $\mathbf{J} \rightarrow \mathbf{0}$. This establishes a *semi-gradient gap*, formally,

Theorem 3 (Semi-Gradient Gap). *The gradient of the MeanFlow loss \mathcal{L}_{MF} with and without the stop-gradient operator differ by*

$$\underbrace{2(t - r) \mathbb{E} \left[\left(\nabla_{\boldsymbol{\theta}} (\partial_{\mathbf{x}_t} \mathbf{u}_{\boldsymbol{\theta}} \cdot \mathbf{v} + \partial_t \mathbf{u}_{\boldsymbol{\theta}}) \right)^{\top} \mathbf{r}_{\boldsymbol{\theta}} \right]}_{\text{mean-field gradient difference}} + \underbrace{\mathbb{E} \left[\nabla_{\boldsymbol{\theta}} \text{Tr}(\mathbf{J} \Sigma_{\mathbf{v}'} \mathbf{J}^{\top}) \right]}_{\text{variance-driven gradient difference}}. \quad (7)$$

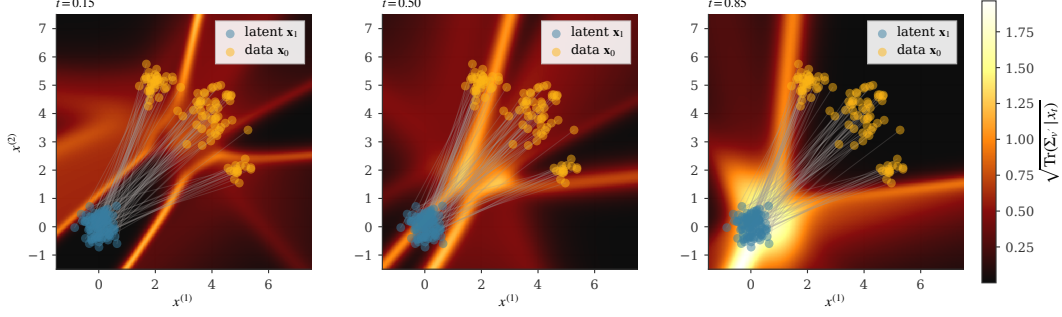


Figure 1: Spatial distribution of $\sqrt{\text{Tr}(\Sigma_{\mathbf{v}'} | \mathbf{x}_t)} = \sqrt{\mathbb{E}_{\mathbf{x}_0 | \mathbf{x}_t} \|\mathbf{v}'\|^2}$ at three timesteps on a two-dimensional Gaussian mixture. Conditional variances concentrate in mode-mixing regions.

In the original MeanFlow, the stop-gradient operator prevents \mathbf{J} from being passed to the optimizer, leading to an empirical non-decreasing loss. Meanwhile, the mean-field difference vanishes at convergence ($\mathbf{r}_\theta \rightarrow \mathbf{0}$) and the variance-driven term $\text{Tr}(\mathbf{J}\Sigma_{\mathbf{v}'}\mathbf{J}^\top)$ dominates. To better illustrate the idea, Figure 1 visualizes the spatial distribution of $\sqrt{\mathbb{E}_{\mathbf{x}_0 | \mathbf{x}_t} \|\mathbf{v}'\|^2}$ on a three-mode, two-dimensional Gaussian mixture. It showcases that the total variance magnitude is non-zero, concentrates in mode-mixing regions where conditional paths overlap, and grows toward the latent endpoint ($t \rightarrow 1$).

3.2 Rethinking tangent as a control variate

The amplification in Theorem 2 arises due to using $\mathbf{v}_{\text{cond}} = \mathbf{v} + \mathbf{v}'$ as the JVP tangent injects the zero-mean fluctuation \mathbf{v}' . Hence, \mathbf{v}_{cond} is analogous to the canonical structure of a Monte Carlo *control variate* [27], where \mathbf{v}_{cond} is a stochastic estimator of the inaccessible \mathbf{v} with known mean, and the coefficient on the noise term \mathbf{v}' determines the bias-variance trade-off. To make this explicit, we introduce a tangent-mixing coefficient $\beta \in [0, 1]$:

$$\tilde{\mathbf{v}}_{\text{tang}}(\beta) \triangleq (1 - \beta) \mathbf{v}_{\text{cond}} + \beta \hat{\mathbf{v}} = \mathbf{v} + (1 - \beta) \mathbf{v}' + \beta \mathbf{b}, \quad (8)$$

where $\hat{\mathbf{v}}$ can be any deterministic proxy for the marginal velocity (e.g., a velocity network) with bias $\mathbf{b} \triangleq \hat{\mathbf{v}} - \mathbf{v}$ that is deterministic given \mathbf{x}_t . Herein, $\beta = 0$ recovers vanilla MeanFlow and $\beta = 1$ replaces the tangent entirely with the deterministic proxy.

Bias-variance trade-off. Substituting $\tilde{\mathbf{v}}_{\text{tang}}(\beta)$ for \mathbf{v}_{cond} in the JVP tangent and propagating through the loss, the per-sample gradient writes

$$\mathbf{g}^{(\beta)} = 2\mathbf{g}^\top \left[\mathbf{r}_\theta + ((1 - \beta)\mathbf{J} - \beta\mathbf{I})\mathbf{v}' + \beta(\mathbf{J} + \mathbf{I})\mathbf{b} \right], \quad (9)$$

where the noise term scales the conditional fluctuation \mathbf{v}' by the matrix $((1 - \beta)\mathbf{J} - \beta\mathbf{I})$, and the bias term scales the proxy error \mathbf{b} by $\beta(\mathbf{J} + \mathbf{I})$. In this case, we can balance the bias-variance trade-off through solving for the optimal coefficient β^* that minimizes the least-squares between the expected per-sample gradient in equation 9 and the target gradients, given by

$$M(\beta) \triangleq \mathbb{E}_{\mathbf{v}' | \mathbf{x}_t} \left[\left\| \mathbf{g}^{(\beta)} - \nabla_\theta \|\mathbf{r}_\theta\|_2^2 \right\|_2^2 \right] = \mathbb{E}_{\mathbf{v}' | \mathbf{x}_t} \left[\left\| \mathbf{g}^{(\beta)} - 2\mathbf{g}^\top \mathbf{r}_\theta \right\|_2^2 \right]. \quad (10)$$

We derive the following theorem.

Theorem 4 (Optimal control-variate coefficient). *Under the scalar-isotropic approximation $\Sigma_{\mathbf{v}'} \approx \sigma^2 \mathbf{I}_d$, $\mathbf{J} \approx \kappa \mathbf{I}_d$, and the parameter-isotropy approximation $\mathbf{g}\mathbf{g}^\top \propto \mathbf{I}_d$ (which reduces M to a per-component MSE; cf. Appendix B),*

$$M(\beta) \propto \beta^2(\kappa + 1)^2 \|\mathbf{b}\|^2 + \sigma^2 d ((1 - \beta)\kappa - \beta)^2. \quad (11)$$

For $\kappa > 0$, $M(\beta)$ admits a unique minimizer

$$\beta^* = \underbrace{\frac{\kappa}{\kappa + 1}}_{\text{noise-cancellation}} \cdot \underbrace{\frac{\sigma^2 d}{\sigma^2 d + \|\mathbf{b}\|^2}}_{\text{shrinkage}}, \quad (12)$$

with optimum value $M(\beta^*) \propto \sigma^2 d \kappa^2 \|\mathbf{b}\|^2 / (\sigma^2 d + \|\mathbf{b}\|^2)$.

Table 1: Concurrent MeanFlow remedies as special cases in our control-variate framework. Each method either drives $\beta \rightarrow 1$ with a deterministic proxy, directly reduces the norm of amplification factor $\|\mathbf{J}\|^2$, or replaces the JVP construction altogether.

| Method | Mechanism in our framework | Practical realization |
|------------------------|---|------------------------------------|
| AlphaFlow [22] | avoid high- κ regimes | α -curriculum schedule |
| Improved MF [23] | deterministic tangent ($\beta \rightarrow 1$) | separate velocity head + sg |
| Modular MF [29] | deterministic tangent ($\beta \rightarrow 1$) | gradient-modulated loss family |
| Kim <i>et al.</i> [30] | deterministic tangent ($\beta \rightarrow 1$) | staged training schedule |
| TVM [25] | remove the spatial Jacobian ($\mathbf{J} \rightarrow \mathbf{0}$) | terminal-time differentiation |
| Re-MeanFlow [24] | reduce $\ \mathbf{J}\ $ | rectified-flow preprocessing |
| Decoupled MF [31] | bypass JVP construction | flow-map conditioning on later t |

See the proof in Appendix B. The two components of β^* play distinct roles: $\kappa/(\kappa+1)$ is the coefficient that *cancels the Jacobian-amplified noise* through destructive interference between the $\mathbf{J}\mathbf{v}'$ and $\mathbf{I}\mathbf{v}'$ contributions in equation 9, while $\sigma^2 d/(\sigma^2 d + \|\mathbf{b}\|^2)$ is the standard James-Stein shrinkage [28] that pulls β^* toward the unbiased corner when the proxy bias $\|\mathbf{b}\|$ is large. Therefore, as the proxy bias shrinks ($\|\mathbf{b}\|^2 \rightarrow 0$), $\beta^* \rightarrow \kappa/(\kappa+1)$, and as the Jacobian magnitude grows ($\kappa \rightarrow \infty$), $\beta^* \rightarrow 1$. Following the theory, we explain the high variance of gradients in the original MeanFlow and establish a connection to practical fixes in concurrent work.

High-variance gradient with suboptimal coefficient. The original MeanFlow uses $\beta = 0$ which is optimal only when $\kappa = 0$ (i.e., $\partial_{\mathbf{x}_t} \mathbf{u}_\theta = \frac{1}{t-r} \mathbf{I}_d$) or when no deterministic proxy is available ($\|\mathbf{b}\| = \infty$). Both conditions fail in practice: trained backbones produce $\partial_{\mathbf{x}_t} \mathbf{u}_\theta$ matrices that are spectrally far from $\frac{1}{t-r} \mathbf{I}_d$, and there are multiple viable deterministic proxies for the marginal \mathbf{v} .

Concurrent works as control variates. Our theory unifies several remedies for MeanFlow’s training pathology across concurrent works into a single one-parameter family. Each empirical fix corresponds to a different practical realization of the optimum β^* , distinguished by *which proxy* they use for \mathbf{v} and *which value of β* the construction implicitly selects. We summarize them in table 1.

4 Related Work

Variance reduction in learning flow-based models. Several recent works address variance in learning flow-based models from complementary perspectives. Stable Velocity [32] reveals a two-regime variance structure in flow matching and proposes composite conditioning; TPC [33] reduces variance through temporal pair coupling; and preconditioned flow matching [34] addresses ill-conditioning via anisotropic preconditioning. Bertrand et al. [35] argue that stochastic-target variance is negligible for standard flow matching, consistent with our analysis, since the problematic amplification we identify is specific to the MeanFlow JVP, not the flow-matching loss itself. Rectified flows [36, 37] reduce trajectory curvature by iterative straightening, which by Theorem 2 reduces $\|\mathbf{J}\|^2$ and hence the amplified noise term.

Control variates and target networks. The control-variate framework we apply has classical roots in Monte Carlo estimation [38]; it is also the analytical structure underlying target networks in deep RL [39] and self-distillation in self-supervised learning [40]. We make the connection explicit by interpreting the EMA-derived tangent in MeanFlow as a target-network-style proxy that drives the control-variate coefficient toward its optimum.

5 Experiments

We empirically validate our theory in Section 3 through probing the bias-variance trade-offs. Specifically, we sweep the tangent-mixing coefficient $\beta \in [0, 1]$ end-to-end and compare the results to the closed-form prediction based on Theorem 4.

Instantiation of the $\beta = 1$ corner. To validate the framework empirically, we need a concrete realization of β that we can sweep at scale. We replace the JVP tangent by an exponential moving-average [41] deterministic proxy $\hat{\mathbf{v}} \leftarrow \mathbf{u}_{\hat{\theta}}(\mathbf{x}_t, t, t)$, and use a small flow-matching loss at $r = t$ to keep the proxy bias $\mathbf{b} = \hat{\mathbf{v}} - \mathbf{v}$ small and bound the bias term $\beta(\mathbf{J} + \mathbf{I})\mathbf{b}$ in equation 9. We keep the regres-

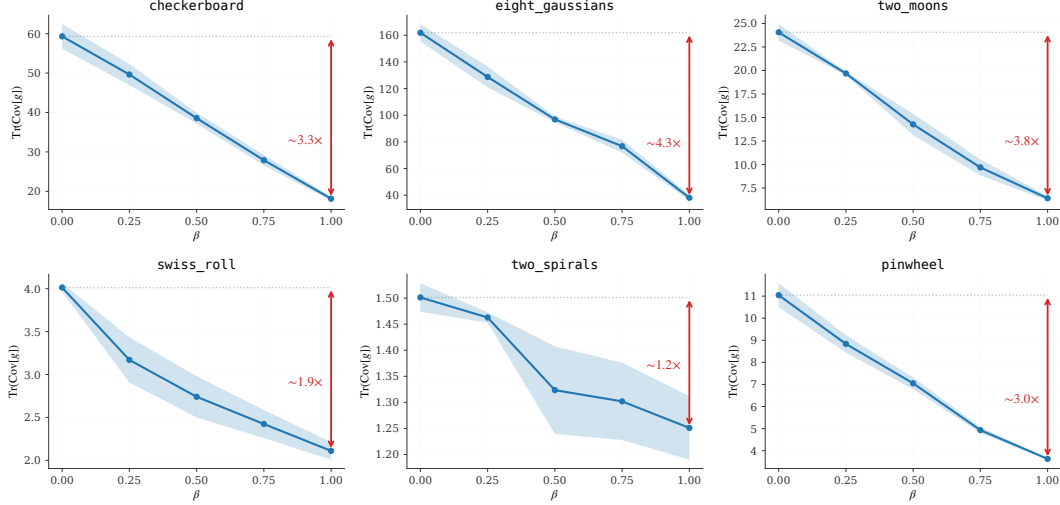


Figure 2: Empirical total gradient variance $\text{Tr}(\text{Cov}[\nabla_{\theta} \ell_{\text{MF}}])$ on six two-dimensional toy datasets with $\beta \in \{0, 0.25, 0.5, 0.75, 1\}$. The monotonic decrease of variances with respect to β on almost every dataset aligns with the prediction in Theorem 2.

sion target \mathbf{v}_{cond} unchanged, exploiting the role asymmetry identified in section 3.1. Appendix C provides details about the full loss, training algorithm, and three propositions characterizing the resulting gradient form, residual bias, and the necessity of the target-tangent role split.

Experiment Setup. We evaluate our theory on three regimes leveraging six two-dimensional toy datasets, dense Gaussian mixtures (DGMM) with various dimensions $d \in \{2, 4, 8, 16, 32, 64\}$, and training DiT-B/4 [42] on ImageNet with Stable Diffusion latents¹. On the 2-D toy and DGMM datasets, we use a three-layer MLP with 128 hidden units, train for 200,000 steps with batch size 256 and three random seeds $\{42, 0, 1\}$, and sweep the eleven-point grid $\beta \in \{0.0, 0.1, \dots, 1.0\}$ for the sample-quality, evaluated by final-step sliced Wasserstein-1 distance (SW_1) on 4096 samples with 500 random projections under a fixed projection seed. On the toy datasets, we additionally run a sub-sweep at $\beta \in \{0, 0.25, 0.5, 0.75, 1\}$ that investigates the per-step total gradient variance $\text{Tr}(\text{Cov}[\nabla_{\theta} \ell_{\text{MF}}])$ using $K = 8$ replica of mini-batches, each with 256 samples, every 2,000 steps and tail-averages over the second half of training. For the DiT, we perform a four-point sweep $\beta \in \{0, 0.25, 0.5, 1\}$ and train the model for 300k steps following the recipe in the original MeanFlow [21]. We defer the full setup, FID table, and direct matrix-form measurement of β^* are to Appendix D.3.

5.1 Variance reduction

Figure 2 reports the total gradient variances $\text{Tr}(\text{Cov}[\nabla_{\theta} \ell_{\text{MF}}])$ on all six 2-D datasets. We observe monotonic decreasing variances with respect to β on almost every dataset. The empirical ordering tracks the variance term $\sigma^2 d((1-\beta)\kappa - \beta)^2$ from Theorem 2 and Theorem 4, empirically validate that the conditional fluctuation \mathbf{v}' is the dominant variance source in the MeanFlow gradients. Meanwhile, we notice that the reduction magnitude varies with the spectral magnitude $\|\mathbf{J}\|$ of the backbone model. The largest reductions appear on the *high-curvature* datasets (e.g., `eight_gaussians`, `checkerboard`), and the smallest (1.20 \times) on `two_spirals`. This is consistent to our theory: low geometric curvature pushes the network toward the flat regime $\partial_{\mathbf{x}_t} \mathbf{u}_{\theta} \rightarrow \frac{1}{t-r} \mathbf{I}_d$, corresponding to $\kappa \approx 0$, and our theorem 4 predicts both a small per-step variance reduction and a left-shift of optimal coefficient $\beta^* \rightarrow 0$ given by the noise-cancellation factor $\kappa/(\kappa+1)$.

5.2 Bias-variance trade-offs

Whereas $\text{Tr}(\text{Cov}[\nabla_{\theta} \ell_{\text{MF}}])$ reveals the variance reduction induced by β , the sample-quality measured by $\text{SW}_1(\beta)$ exposes the full bias-variance trade-off. Figure 3 traces $\text{SW}_1(\beta)$ across the full 11-point

¹<https://huggingface.co/enterprise-explorers/sd-vae-ft-mse-flax>

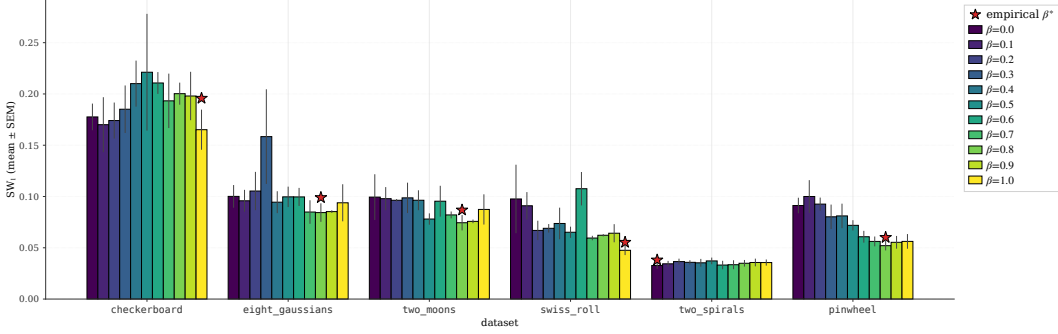


Figure 3: Empirical sample-quality measured by sliced Wasserstein-1 distance $SW_1(\beta)$ on six 2-D toy datasets with $\beta \in \{0.0, 0.1, \dots, 1.0\}$. Bars are grouped by dataset and colored by β with standard error bar. The red star marks the empirical optimal coefficient β^* . Five of six datasets settle at $\beta^* \in \{0.8, 1.0\}$ near the deterministic-tangent corner; `two_spirals` alone settles at $\beta^* = 0$.

Table 2: DGMM β -sweep summary across dimensions $d \in \{2, 4, 8, 16, 32, 64\}$. The quality gap column marks reduction that exceed one standard error mean with \dagger . SW_1 is essentially β -insensitive at $d \leq 32$, while only $d=64$ shows a tentative interior minimum.

| d | $SW_1(\beta=0)$ | $SW_1(\beta=\beta^*)$ | Quality Gap | β^* |
|-----|-------------------|-----------------------|--------------------|-----------|
| 2 | 0.152 ± 0.022 | 0.146 ± 0.015 | $\sim 4\%$ | 1.0 |
| 4 | 0.083 ± 0.011 | 0.083 ± 0.011 | $< 1\%$ | 0.8 |
| 8 | 0.062 ± 0.003 | 0.062 ± 0.003 | $\sim 1\%$ | 1.0 |
| 16 | 0.044 ± 0.002 | 0.044 ± 0.003 | $< 1\%$ | 1.0 |
| 32 | 0.034 ± 0.001 | 0.033 ± 0.001 | $< 1\%$ | 0.1 |
| 64 | 0.028 ± 0.003 | 0.025 ± 0.001 | $\sim 9\%^\dagger$ | 0.4 |

grid on six 2-D toy datasets. On the five high-curvature datasets, the empirical β^* falls in between $\{0.8, 1.0\}$, recovering the predicted $\beta \rightarrow 1$ location with a small bias norm $\|\mathbf{b}\|_2^2$ when the EMA proxy is accurate. On the lower-curvature `two_spirals` dataset, consistent with section 5.1, the geometry drives $\partial_{x_i} \mathbf{u}_\theta \rightarrow \frac{1}{i-r} \mathbf{I}_d$, essentially pushing κ toward zero. The predicted β^* then shrinks toward the unbiased corner $\beta = 0$ through the noise-cancellation factor $\kappa/(\kappa+1)$ in Theorem 4, and the empirical sweep result concurs. Meanwhile, we are surprised that the $\beta^* = 1$ instantiation reduces SW_1 by 54% compared to the original MeanFlow ($\beta = 0$) on the `swiss_roll` dataset.

5.3 Scaling with feature dimensions

We investigate whether our theory holds with increasing in feature dimensions by sweeping the coefficient $\beta \in \{0, 0.1, \dots, 1\}$ on dense Gaussian mixture (DGMM) datasets in \mathbb{R}^d , varying $d \in \{2, 4, 8, 16, 32, 64\}$. Table 2 summarizes the sample-quality gap between the original MeanFlow with $\beta=0$ and the empirical β^* at each d . We report full results in Table 5 of Appendix D. On low-dimensional datasets with $d \in \{2, 4, 8, 16, 32\}$, SW_1 is essentially β -insensitive, where the quality gap between $\beta=0$ and β^* stays within one standard error of the mean (SEM). This is consistent with the prediction from theorem 4 when the EMA proxy yields small $\|\mathbf{b}\|_2^2$. The noise-cancellation factor $\kappa/(\kappa+1)$ saturates near 1 across the whole β range, leading to flat $SW_1(\beta)$. At $d=64$ the data hints at an interior minimum at $\beta^* = 0.4$ with a $\sim 9\%$ reduction over $\beta=0$, consistent with κ coming off saturation with increasing data dimension d . In the following section 5.4, we will showcase that the same observation is consistent with larger and more complicated DiT model, where $\beta_{\text{matrix}}^* \approx 0.94$ also sits short of the deterministic-tangent corner.

5.4 Latent Diffusion Transformers on ImageNet

We further investigate whether our theory generalizes to large model with high-dimensional features. Figure 4 shows two complementary measurements from the experiments with DiT-B/4 on ImageNet. The left panel in Figure 4 validates that the gradient-variance reduction predicted by Theorem 2 car-

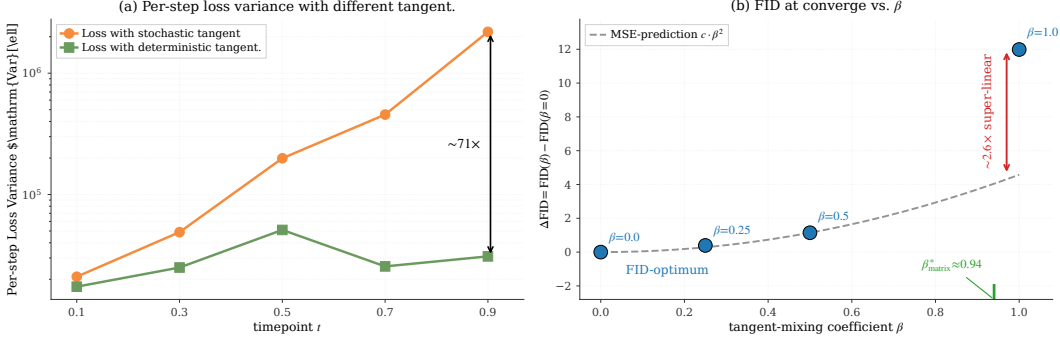


Figure 4: Experiment results training DiT-B/4 on ImageNet-256. *Left*: Per-step loss variance under the stochastic ($\beta = 0$) versus deterministic ($\beta = 1$) tangent, measured on the baseline ($\beta = 0$) checkpoint with the same data and noise. The deterministic-tangent variance is roughly t -flat while the stochastic-tangent variance grows by two orders of magnitude with t , confirming the Jacobi-factor amplification of Theorem 2. *Right*: FID at converge with respect to different β . We report empirical $\Delta\text{FID}(\beta) = \text{FID}(\beta) - \text{FID}(\beta = 0)$ at the matched training step 295k with different β . The dashed gray curve is the quadratic $c\beta^2$. The FID at converge with $\beta = 1$ sits a factor of ~ 2.6 above the quadratic curve, indicating a super-linear relationship between the FID and the bias. The optimal coefficient calculated in matrix form is $\beta_{\text{matrix}}^* \approx 0.94$.

ries over from 2-D toy benchmark datasets to DiT. Herein, we directly measure the per-step loss variance using the model trained with the original MeanFlow loss, using two distinct tangents: the stochastic conditional-velocity tangent \mathbf{v}_{cond} and the deterministic EMA tangent $\mathbf{u}_{\theta}(\mathbf{x}_t, t, t)$. We observe that the loss variance with deterministic-tangent stays roughly flat across t , while the stochastic-tangent variance grows by two orders of magnitude. The widening gap directly validates the Jacobi-factor amplification of Theorem 2, where the stochastic tangent passes the conditional-velocity noise through $\mathbf{J} = (t-r)\partial_{\mathbf{x}_t}\mathbf{u} - \mathbf{I}$, which the deterministic tangent eliminates by construction. We observe the same pattern using checkpoint of the $\beta = 1$ instantiation (see appendix D.3), confirming that the amplification is a property of the architecture and data.

The right panel in Figure 4 visualizes the FID at converge as a function of β , with y -axis the empirical $\Delta\text{FID}(\beta) \triangleq \text{FID}(\beta) - \text{FID}(\beta = 0)$. The result shows that an ordering of $\text{FID}(\beta = 0) < \text{FID}(\beta = 0.25) < \text{FID}(\beta = 0.5) < \text{FID}(\beta = 1)$ holds at matched-step checkpoints. We report per-checkpoint values in Table 6 of Appendix D.3. The result establishes the following observation:

FID-MSE landscape mismatch. We report the direct measurement of both ingredients in Theorem 4 on the DiT checkpoints, including the EMA-tracking proxy $\|\widehat{\mathbf{b}}\|^2$ and the irreducible noise floor $\sigma^2 d$, in Appendix D.3. The result predicts an optimal β^* in the interior range $[0.46, 0.50]$ under the scalar-isotropic approximation, while the matrix-form β_{matrix}^* is even larger (see below). The empirical ordering of FID at convergence is hence consistent with the prediction. To test whether FID tracks the gradient-MSE *quantitatively*, we fit a MSE-prediction curve $c\beta^2$ and compare the $\beta = 1$ offset, where c is given by

$$c \leftarrow \arg \min_{c \in \mathbb{R}} \|\Delta\text{FID}(\beta) - c\beta^2\|_2^2, \quad \beta \in \{0.0, 0.25, 0.5\}. \quad (13)$$

Figure 4 shows a $\sim 2.6\times$ super-linear amplification along the ΔFID axis, indicating that the FID over-penalizes bias relative to gradient MSE. As a consequence, the FID-optimal β shifts past the gradient-MSE interior minimizer all the way to the unbiased corner $\beta = 0$.

To verify that our isotropic approximation in theorem 4 is not artifactual, we directly measured a matrix-form upper bound on β_{matrix}^* on the baseline checkpoint by sampling actual \mathbf{v}' values from the conditional distribution (see Appendix B). The estimator omits the bias term $\|(\mathbf{J} + \mathbf{I})\mathbf{b}\|^2$ from the denominator, giving

$$\beta_{\text{no bias}}^* \triangleq \frac{\text{Tr}(\mathbf{J}\Sigma_{\mathbf{v}'}(\mathbf{J} + \mathbf{I})^\top)}{\text{Tr}((\mathbf{J} + \mathbf{I})\Sigma_{\mathbf{v}'}(\mathbf{J} + \mathbf{I})^\top)} \geq |\beta_{\text{matrix}}^*|, \quad (14)$$

since the omitted bias term is *non-negative*. We evaluate the bound at $t \in \{0.1, 0.3, 0.5, 0.7, 0.9\}$ with fixed gap $t - r = 0.25$, and 512 samples per t using $\mathbf{u}_{\theta}(\mathbf{x}_t, t, t)$ as the marginal-velocity proxy. The numerator is *strictly positive* at every probed t , ruling out the unbiased-corner regime

$\beta_{\text{matrix}}^* \leq 0$. Aggregated across t , we have $\beta_{\text{no bias}}^* \approx 0.94$, which is close to the deterministic-tangent corner and *larger* than the scalar-isotropic estimate $\beta^* \in [0.46, 0.50]$. The full β_{matrix}^* then lies in $(0, 0.94]$. Herein, we do not pin down the exact value due to the inaccessible true model bias $\mathbf{b} = \mathbf{u}_\theta(\mathbf{x}_t, t, t) - \mathbf{v}(\mathbf{x}_t, t)$ on ImageNet without access to the conditional distribution $p(\mathbf{x}_0 | \mathbf{x}_t)$. The matrix-form measurement further strengthens, rather than weakens, the FID-MSE mismatch: the gradient-MSE optimum sits in $(0, 0.94]$ while the FID optimum sits at the unbiased corner $\beta = 0$.

6 Conclusion

In this paper, we establish a theory from the perspective of Monte Carlo control variates that isolates the statistical structure of training pathology in the original MeanFlow. We identify two distinct roles the conditional velocity plays in the loss, and the original objective assigns the wrong coefficient to one of them. Following the theory, we derive the optimal tangent-mixing coefficient for the control variate in closed form. In our experiment, we conduct a controlled sweep of the coefficient to recover the predicted bias-variance trade-offs, scaling from two-dimensional toy datasets to a large-scale DiT-B/4 model on ImageNet-256 scale. In addition, our experiment with DiT reveals a quantitative *FID-MSE landscape mismatch*, where the optimal coefficient given by minimizing matrix-form MSE sits at $\beta^* \approx 0.94$ while the optimal coefficient minimizing the FID leans towards the unbiased corner $\beta = 0$, with a super-linear relationship between the empirical $\text{FID}(\beta = 1)$ and the bias. We discuss practical insights and limitations below.

Practical insights. Our Theorem 4 predicts two factors that determines the empirical β^* through the data-dependent κ and model bias $\|\mathbf{b}\|^2$. Selecting the appropriate β reflects the balance between bias and variance. Thereby, when gradient stability is the primary concern, we recommend toggling β toward the corner $\kappa/(\kappa+1)$, which is attainable through an EMA proxy $\mathbf{u}_{\bar{\theta}}(\mathbf{x}, t)$ with $O(1)$. When sample quality is the primary metric, our DiT experiment suggests toggling β back toward 0 or annealing β with respect to $\|\mathbf{b}\|_2^2$ until the FID bias penalty becomes negligible. A metric-aware β schedule that interpolates between these regimes during training is a promising direction for future work.

Limitations. We acknowledge several limitations of this work: (i) *Scalar-isotropic approximation.* Our Theorem 4 is derived under $\mathbf{J} \approx \kappa \mathbf{I}_d$ and $\Sigma_{\mathbf{v}'} \approx \sigma^2 \mathbf{I}_d$. In the full diagonal matrix-valued setting the optimum is direction-dependent: a per-direction $\beta_i = \frac{\mathbf{J}_{ii}}{\mathbf{J}_{ii+1}} \cdot \frac{\sigma_i^2}{\sigma_i^2 + b_i^2}$ would minimize the per-component gradient MSE, and a single global β trades off residual variance across directions. This assumption may be valid for backbones whose Jacobian spectrum is concentrated, but it may fail for more complex models or highly anisotropic data. (ii) *FID-aware loss design.* Our experiment characterizes the FID-MSE mismatch but does not derive an FID-aware loss or β schedule, which remains an open question. (iii) *Non-Euclidean data.* We conduct our experiment in the Euclidean space \mathbb{R}^d . Extending the closed-form β^* to manifold MeanFlow [43] is straightforward at the gradient level but requires care in defining the second moment $\text{Tr}(\Sigma_{\mathbf{v}'})$ on tangent spaces.

Future work. There are three promising future directions. First, we argue that our control-variate diagnosis applies to any self-supervised one-step generative model that bootstraps a parametrized map as the JVP-style total derivative in MeanFlow, including consistency models [18] and shortcut models [44]. Meanwhile, a per-sample scalar coefficient driven by online estimates of κ and $\|\mathbf{b}\|_2^2$ can potentially close the global-vs-per-sample and the scalar-vs-matrix gap during training. Last but not least, an adaptive schedule that interpolates between the gradient-MSE optimum and the FID-optimal corner, calibrated by either a learned proxy or proxy-quality validation FID, could resolve the FID-MSE mismatch we identified.

References

- [1] Jonathan Ho, Ajay Jain, and Pieter Abbeel. Denoising diffusion probabilistic models. In H. Larochelle, M. Ranzato, R. Hadsell, M.F. Balcan, and H. Lin, editors, *Advances in Neural Information Processing Systems*, volume 33, pages 6840–6851. Curran Associates, Inc., 2020.
- [2] Yang Song, Jascha Sohl-Dickstein, Diederik P. Kingma, Abhishek Kumar, Stefano Ermon, and Ben Poole. Score-based generative modeling through stochastic differential equations. In *International Conference on Learning Representations*, 2021.
- [3] Tero Karras, Miika Aittala, Timo Aila, and Samuli Laine. Elucidating the design space of diffusion-based generative models. In *Advances in Neural Information Processing Systems*, volume 35, 2022.

- [4] Prafulla Dhariwal and Alexander Nichol. Diffusion models beat GANs on image synthesis. In *Advances in Neural Information Processing Systems*, volume 34, 2021.
- [5] Patrick Esser, Sumith Kulal, Andreas Blattmann, Rahim Entezari, Jonas Müller, Harry Saini, Yam Levi, Dominik Lorenz, Naveen Rafi, Tim Shafir, et al. Scaling rectified flow transformers for high-resolution image synthesis. In *Proceedings of the 41st International Conference on Machine Learning*, volume 235 of *Proceedings of Machine Learning Research*, 2024.
- [6] Ricky T. Q. Chen, Yulia Rubanova, Jesse Bettencourt, and David K. Duvenaud. Neural ordinary differential equations. In *Advances in Neural Information Processing Systems*, volume 31, 2018.
- [7] Danilo Rezende and Shakir Mohamed. Variational inference with normalizing flows. In *Proceedings of the 32nd International Conference on Machine Learning*, volume 37 of *Proceedings of Machine Learning Research*, pages 1530–1538, 2015.
- [8] Laurent Dinh, Jascha Sohl-Dickstein, and Samy Bengio. Density estimation using Real-NVP. In *International Conference on Learning Representations*, 2017.
- [9] Will Grathwohl, Ricky T. Q. Chen, Jesse Bettencourt, Ilya Sutskever, and David Duvenaud. FFJORD: Free-form continuous dynamics for scalable reversible generative models. In *International Conference on Learning Representations*, 2019.
- [10] Yaron Lipman, Ricky T. Q. Chen, Heli Ben-Hamu, Maximilian Nickel, and Matt Le. Flow matching for generative modeling, 2023.
- [11] Alexander Tong, Kilian Fatras, Nikolay Malkin, Guillaume Hugué, Yanlei Zhang, Jarrid Rector-Brooks, Guy Wolf, and Yoshua Bengio. Improving and generalizing flow-based generative models with minibatch optimal transport, 2024.
- [12] Michael S. Albergo and Eric Vanden-Eijnden. Building normalizing flows with stochastic interpolants, 2023.
- [13] Michael Albergo, Nicholas M. Boffi, and Eric Vanden-Eijnden. Stochastic interpolants: A unifying framework for flows and diffusions. *Journal of Machine Learning Research*, 26(209):1–80, 2025.
- [14] Yang Song and Stefano Ermon. Generative modeling by estimating gradients of the data distribution. In *Advances in Neural Information Processing Systems*, volume 32, 2019.
- [15] Tim Salimans and Jonathan Ho. Progressive distillation for fast sampling of diffusion models, 2022.
- [16] Tianwei Yin, Michaël Gharbi, Richard Zhang, Eli Shechtman, Frédo Durand, William T. Freeman, and Taesung Park. One-step diffusion with distribution matching distillation. In *Proceedings of the IEEE/CVF Conference on Computer Vision and Pattern Recognition (CVPR)*, pages 6613–6623, June 2024.
- [17] Tianwei Yin, Michaël Gharbi, Taesung Park, Richard Zhang, Eli Shechtman, Frédo Durand, and William T. Freeman. Improved distribution matching distillation for fast image synthesis. In A. Globerson, L. Mackey, D. Belgrave, A. Fan, U. Paquet, J. Tomczak, and C. Zhang, editors, *Advances in Neural Information Processing Systems*, volume 37, pages 47455–47487. Curran Associates, Inc., 2024.
- [18] Yang Song, Prafulla Dhariwal, Mark Chen, and Ilya Sutskever. Consistency models. In *Proceedings of the 40th International Conference on Machine Learning*, ICML’23. JMLR.org, 2023.
- [19] Cheng Lu and Yang Song. Simplifying, stabilizing and scaling continuous-time consistency models, 2025.
- [20] Nicholas M. Boffi, Michael S. Albergo, and Eric Vanden-Eijnden. Flow map matching with stochastic interpolants: A mathematical framework for consistency models, 2025.
- [21] Zhengyang Geng, Mingyang Deng, Xingjian Bai, J. Zico Kolter, and Kaiming He. Mean flows for one-step generative modeling, 2025.
- [22] Huijie Zhang, Aliaksandr Siarohin, Willi Menapace, Michael Vasilkovsky, Sergey Tulyakov, Qing Qu, and Ivan Skorokhodov. Alphaflow: Understanding and improving meanflow models, 2025.
- [23] Zhengyang Geng, Yiyang Lu, Zongze Wu, Eli Shechtman, J. Zico Kolter, and Kaiming He. Improved mean flows: On the challenges of fastforward generative models, 2025.
- [24] Xinxi Zhang, Shiwei Tan, Quang Nguyen, Quan Dao, Ligong Han, Xiaoxiao He, Tunyu Zhang, Chengzhi Mao, Dimitris Metaxas, and Vladimir Pavlovic. Overcoming the curvature bottleneck in meanflow, 2026.

- [25] Linqi Zhou, Mathias Parger, Ayaan Haque, and Jiaming Song. Terminal velocity matching, 2026.
- [26] Zhiqi Li, Yuchen Sun, Greg Turk, and Bo Zhu. Functional mean flow in hilbert space, 2025.
- [27] Paul Glasserman. *Monte Carlo methods in financial engineering*, volume 53. Springer New York, NY, 2003.
- [28] William James, Charles Stein, et al. Estimation with quadratic loss. In *Proceedings of the fourth Berkeley symposium on mathematical statistics and probability*, volume 1, pages 361–379. University of California Press, 1961.
- [29] Haochen You, Baojing Liu, and Hongyang He. Modular meanflow: Towards stable and scalable one-step generative modeling, 2025.
- [30] Jin-Young Kim, Hyojun Go, Lea Bogensperger, Julius Erbach, Nikolai Kalischek, Federico Tombari, Konrad Schindler, and Dominik Narnhofer. Understanding, accelerating, and improving meanflow training, 2025.
- [31] Kyungmin Lee, Sihyun Yu, and Jinwoo Shin. Decoupled meanflow: Turning flow models into flow maps for accelerated sampling, 2025.
- [32] Donglin Yang, Yongxing Zhang, Xin Yu, Liang Hou, Xin Tao, Pengfei Wan, Xiaojuan Qi, and Renjie Liao. Stable velocity: A variance perspective on flow matching, 2026.
- [33] Chika Maduabuchi and Jindong Wang. Temporal pair consistency for variance-reduced flow matching, 2026.
- [34] Shadab Ahamed, Eshed Gal, Simon Ghyselincks, Md Shahriar Rahim Siddiqui, Moshe Eliasof, and Eldad Haber. Preconditioned score and flow matching, 2026.
- [35] Quentin Bertrand, Anne Gagneux, Mathurin Massias, and Rémi Emonet. On the closed-form of flow matching: Generalization does not arise from target stochasticity, 2025.
- [36] Xingchao Liu, Chengyue Gong, and Qiang Liu. Flow straight and fast: Learning to generate and transfer data with rectified flow, 2022.
- [37] Sangyun Lee, Zinan Lin, and Giulia Fanti. Improving the training of rectified flows. In A. Globerson, L. Mackey, D. Belgrave, A. Fan, U. Paquet, J. Tomczak, and C. Zhang, editors, *Advances in Neural Information Processing Systems*, volume 37, pages 63082–63109. Curran Associates, Inc., 2024.
- [38] Peter W. Glynn and Roberto Szechtman. Some new perspectives on the method of control variates. *Monte Carlo and Quasi-Monte Carlo Methods 2000*, pages 27–49, 2002.
- [39] Volodymyr Mnih, Koray Kavukcuoglu, David Silver, et al. Human-level control through deep reinforcement learning. *Nature*, 518:529–533, 2015.
- [40] Jean-Bastien Grill, Florian Strub, Florent Altché, et al. Bootstrap your own latent: A new approach to self-supervised learning. In *NeurIPS*, 2020.
- [41] Boris T. Polyak and Anatoli B. Juditsky. Acceleration of stochastic approximation by averaging. *SIAM Journal on Control and Optimization*, 30(4):838–855, 1992.
- [42] William Peebles and Saining Xie. Scalable diffusion models with transformers. In *Proceedings of the IEEE/CVF International Conference on Computer Vision (ICCV)*, pages 4195–4205, 2023.
- [43] Dongyeop Woo, Marta Skreta, Seonghyun Park, Kirill Neklyudov, and Sungsoo Ahn. Riemannian mean-flow, 2026.
- [44] Kevin Frans, Danijar Hafner, Sergey Levine, and Pieter Abbeel. One step diffusion via shortcut models, 2025.

Supplementary Material

| | | |
|----------|---|-----------|
| A | Notations | 13 |
| B | Proofs | 14 |
| B.1 | Proof of Lemma 1 | 14 |
| B.2 | Proof of Theorem 2 (Jacobian Variance Amplification) | 14 |
| B.3 | Proof of Theorem 3 (Semi-Gradient Gap) | 15 |
| B.4 | Proof of Theorem 4 (Optimal Control-Variate Coefficient) | 15 |
| B.5 | Proof of Proposition 1 (Gradient under the $\beta = 1$ corner loss) | 17 |
| B.6 | Proof of Proposition 2 (Bias-Variance Tradeoff) | 17 |
| B.7 | Proof of Proposition 3 (Target/Tangent Bias Asymmetry) | 17 |
| C | Implementation Details | 18 |
| D | Additional Results | 19 |
| D.1 | 2-D Toy Benchmark | 19 |
| D.2 | Full β -sweep grid on DGMM | 19 |
| D.3 | Latent DiT-B/4 on ImageNet-256 | 20 |

A Notations

To promote the readability of our readers, table 3 lists all the notations we use in this work.

Table 3: Table of notations.

| Notation | Description |
|--|--|
| <i>Scalars</i> | |
| d | Dimension of the data samples |
| p | Number of parameters in the model |
| c | Coefficient in the fitted gradient-MSE curve $c\beta^2$ |
| <i>State vectors and velocity fields</i> | |
| \mathbf{x}, \mathbf{x}_t | Random data sample / state at interpolant time t |
| \mathbf{x}, \mathbf{x}_t | Realized state / state at time t |
| $\mathbf{v}(\mathbf{x}, t)$ | Marginal velocity field |
| \mathbf{v}_{cond} | Conditional velocity $\mathbf{v}_{\text{cond}} \triangleq \mathbf{v}(\mathbf{x}, t \mathbf{x}_0)$. |
| \mathbf{v}' | Conditional velocity fluctuation: $\mathbf{v}' = \mathbf{v}_{\text{cond}} - \mathbf{v}(\mathbf{x}, t)$ |
| $\hat{\mathbf{v}}$ | Deterministic proxy for the marginal velocity field \mathbf{v} |
| <i>Model</i> | |
| $\mathbf{u}_\theta(\mathbf{x}, r, t)$ | Two-parameter average velocity field with parameters θ |
| $\mathbf{u}_{\bar{\theta}}$ | Copy of \mathbf{u}_θ with exponential moving-average parameters $\bar{\theta}$ |
| <i>Spatial-Jacobian quantities</i> | |
| $\partial_{\mathbf{x}_t} \mathbf{u}_\theta$ | Spatial Jacobian of \mathbf{u}_θ with respect to state \mathbf{x}_t |
| \mathbf{J} | Jacobi factor: $\mathbf{J} = (t - r) \partial_{\mathbf{x}_t} \mathbf{u}_\theta - \mathbf{I}_d \in \mathbb{R}^{d \times d}$ |
| \mathbf{A} | Shorthand $\mathbf{A} \triangleq \mathbf{J} + \mathbf{I}_d = (t - r) \partial_{\mathbf{x}_t} \mathbf{u}_\theta$ |
| κ | Scalar-isotropic approximation for \mathbf{J} : $\mathbf{J} \approx \kappa \mathbf{I}_d$ |
| <i>Bias and Variances</i> | |
| $\Sigma_{\mathbf{v}'}$ | Covariance matrix of conditional velocity fluctuation: $\text{Cov}_{\mathbf{x}_0 \mathbf{x}_t}[\mathbf{v}']$ |
| $\sigma^2 d$ | Total variance of \mathbf{v}' in scalar-isotropic case: $\Sigma_{\mathbf{v}'} \approx \sigma^2 \mathbf{I}_d$ |
| \mathbf{b} | Proxy bias: $\mathbf{b} \triangleq \hat{\mathbf{v}} - \mathbf{v}(\mathbf{x}_t, t)$ |
| $\ \widehat{\mathbf{b}}\ _2^2$ | EMA-tracking proxy for bias: $\ \widehat{\mathbf{b}}\ _2^2 \triangleq \mathbb{E}_{\mathbf{x}_t} [\ \mathbf{u}_\theta(\mathbf{x}_t, t, t) - \mathbf{u}_{\bar{\theta}}(\mathbf{x}_t, t, t)\ ^2]$ |
| <i>Gradients</i> | |
| $\nabla_{\theta} \ell_{\text{MF}}$ | Per-step gradient of the MeanFlow loss |
| \mathbf{g} | Parameter Jacobian of the network output: $\mathbf{g} \triangleq \nabla_{\theta} \mathbf{u}_\theta \in \mathbb{R}^{d \times p}$ |
| \mathbf{G}_θ | Parameter-space Gram matrix: $\mathbf{G}_\theta \triangleq \mathbf{g} \mathbf{g}^\top \in \mathbb{R}^{d \times d}$ |
| <i>Tangent-mixing coefficient</i> | |
| $\beta \in [0, 1]$ | Tangent-mixing coefficient defined in equation 8 |
| β^* | Closed-form scalar-isotropic minimizer of $M(\beta)$ in theorem 4 |
| β_{matrix}^* | Matrix-form minimizer in appendix B, equation 30 |
| $M(\beta)$ | Conditional MSE of the per-sample gradient equation 9 at coefficient β |
| <i>Loss components</i> | |
| \mathcal{L}_{MF} | Vanilla MeanFlow loss defined by equation 4 |
| $\mathcal{L}_{\text{MF}}^{\text{EMA}}$ | EMA-tangent variant of the MeanFlow loss defined by equation 38 |
| \mathcal{L}_{FM} | Flow-matching anchor loss defined by equation 39 |
| $\mathcal{L}_{\beta=1}$ | $\beta = 1$ corner training loss defined by equation 40 |
| <i>Operators</i> | |
| $\text{sg}[\cdot]$ | Stop-gradient operator |
| $\text{JVP}(\mathbf{u}, \mathbf{x}, \mathbf{v})$ | Jacobian-vector product of \mathbf{u} evaluated at \mathbf{x} in tangent direction \mathbf{v} |
| $\text{Tr}(\cdot), \text{Cov}[\cdot], \text{Var}[\cdot]$ | Trace, covariance, variance |
| $\text{div}(\mathbf{f})$ | Divergence of vector field \mathbf{f} |

B Proofs

B.1 Proof of Lemma 1

Lemma 1. *Given vector fields \mathbf{v}_{cond} generating conditional probability paths $p(\mathbf{x}, t | \mathbf{x}_0)$, for any $\mathbf{x}_0 \sim p(\mathbf{x}_0)$, the expected conditional velocity field is equal to the marginal velocity field*

$$\mathbf{v}(\mathbf{x}, t) = \mathbb{E}_{\mathbf{x}_0 \sim p(\mathbf{x}_0 | \mathbf{x}_t = \mathbf{x})}[\mathbf{v}(\mathbf{x}, t | \mathbf{x}_0)].$$

Proof. We follow the standard flow-matching construction [1, 2]. A sufficient and necessary condition for a velocity field $\mathbf{v}(\mathbf{x}, t)$ to generate a probability density path is given by the continuity equation [3], which writes:

$$\frac{\partial}{\partial t} p(\mathbf{x}, t) + \text{div}(p(\mathbf{x}, t)\mathbf{v}(\mathbf{x}, t)) = 0. \quad (15)$$

Meanwhile, by the law of total probability and the definition of the conditional velocity field,

$$p(\mathbf{x}, t) = \int_{\mathcal{X}} p(\mathbf{x}, t | \mathbf{x}_0) p(\mathbf{x}_0) d\mathbf{x}_0, \quad \forall p(\mathbf{x}_0). \quad (16)$$

Taking the derivative with respect to time step t on both sides and applying Bayes' rule yields

$$\begin{aligned} \frac{\partial}{\partial t} p(\mathbf{x}, t) &= \int_{\mathcal{X}} \frac{\partial}{\partial t} p(\mathbf{x}, t | \mathbf{x}_0) p(\mathbf{x}_0) d\mathbf{x}_0 \\ &= \int_{\mathcal{X}} -\text{div}(p(\mathbf{x}, t | \mathbf{x}_0)\mathbf{v}(\mathbf{x}, t | \mathbf{x}_0)) \cdot p(\mathbf{x}_0) d\mathbf{x}_0 \\ &= -\text{div} \cdot \left(\int_{\mathcal{X}} \mathbf{v}(\mathbf{x}, t | \mathbf{x}_0) \cdot p(\mathbf{x}, t) \cdot p(\mathbf{x}_0 | \mathbf{x}_t = \mathbf{x}) d\mathbf{x}_0 \right) \\ &= -\text{div}(p(\mathbf{x}, t)\mathbb{E}_{\mathbf{x}_0 \sim p(\mathbf{x}_0 | \mathbf{x}_t = \mathbf{x})}[\mathbf{v}(\mathbf{x}, t | \mathbf{x}_0)]). \end{aligned} \quad (17)$$

Combining equation 15 and equation 17 recovers the relationship. Proof completes. \square

B.2 Proof of Theorem 2 (Jacobian Variance Amplification)

Theorem 2 (Jacobian Variance Amplification). *Let $\mathbf{g} \triangleq \nabla_{\theta} \mathbf{u}_{\theta}(\mathbf{x}_t, r, t) \in \mathbb{R}^{d \times p}$ be the parameter Jacobian of the average velocity. The trace of the conditional gradient covariance (i.e., the total variance) of $\ell_{\text{MF}}(\theta)$ in equation 4 satisfies*

$$\text{Tr}(\text{Cov}[\nabla_{\theta} \ell_{\text{MF}} | \mathbf{x}_t]) \propto \text{Tr}(\mathbf{g}^{\top} \mathbf{J} \Sigma_{\mathbf{v}'} \mathbf{J}^{\top} \mathbf{g}).$$

Proof. By substituting $\mathbf{v}_{\text{cond}} = \mathbf{v}(\mathbf{x}, t) + \mathbf{v}'$, the per-step loss ℓ_{MF} expands:

$$\begin{aligned} \ell_{\text{MF}} &= \|\mathbf{u}_{\theta} + (t - r) \text{sg}[\text{JVP}(\mathbf{u}_{\theta}, (\mathbf{x}_t, r, t), (\mathbf{v}_{\text{cond}}, 0, 1))] - \mathbf{v}_{\text{cond}}\|_2^2 \\ &= \|\mathbf{u}_{\theta} + (t - r) \text{sg}[\partial_{\mathbf{x}_t} \mathbf{u}_{\theta} \cdot \mathbf{v}(\mathbf{x}, t) + \partial_t \mathbf{u}_{\theta}] - \mathbf{v}(\mathbf{x}, t) + [(t - r)\partial_{\mathbf{x}_t} \mathbf{u}_{\theta} - \mathbf{I}_d] \mathbf{v}'\|_2^2 \\ &= \|\mathbf{r}_{\theta}^{\text{sg}} + \mathbf{J} \mathbf{v}'\|_2^2, \end{aligned} \quad (18)$$

where $\mathbf{r}_{\theta}^{\text{sg}}$ is the mean-field residual and $\mathbf{J} = (t - r)\partial_{\mathbf{x}_t} \mathbf{u}_{\theta} - \mathbf{I}_d$ is the Jacobi factor. With the stop-gradient operator, the gradient of the per-sample loss passes through only the mean-field residual $\mathbf{r}_{\theta}^{\text{sg}}$. Let $\mathbf{g} \triangleq \nabla_{\theta} \mathbf{u}_{\theta} \in \mathbb{R}^{d \times p}$ denote the parameter Jacobian of the network output. The per-step gradient is then given by

$$\nabla_{\theta} \ell_{\text{MF}} = 2\mathbf{g}^{\top} (\mathbf{r}_{\theta}^{\text{sg}} + \mathbf{J} \mathbf{v}'), \quad (19)$$

where all three quantities (\mathbf{g} , $\mathbf{r}_{\theta}^{\text{sg}}$, and \mathbf{J}) are deterministic conditioned on \mathbf{x}_t . Since $\mathbb{E}_{\mathbf{x}_0 | \mathbf{x}_t}[\mathbf{v}'] = \mathbf{0}$ by equation 1, the conditional mean gradient then writes

$$\mathbb{E}[\nabla_{\theta} \ell | \mathbf{x}_t] = 2\mathbf{g}^{\top} (\mathbf{r}_{\theta}^{\text{sg}} + \mathbf{0}) = 2\mathbf{g}^{\top} \mathbf{r}_{\theta}^{\text{sg}}. \quad (20)$$

The centered gradient is $\nabla_{\theta}\ell - \mathbb{E}[\nabla_{\theta}\ell \mid \mathbf{x}_t] = 2(\nabla_{\theta}\mathbf{u}_{\theta})^{\top} \mathbf{J}\mathbf{v}'$, so the conditional variance is:

$$\begin{aligned} \text{Var}[\nabla_{\theta}\ell \mid \mathbf{x}_t] &= \mathbb{E}\left[\|2(\nabla_{\theta}\mathbf{u}_{\theta})^{\top} \mathbf{J}\mathbf{v}'\|^2 \mid \mathbf{x}_t\right] \\ &= 4 \mathbb{E}\left[\left(\mathbf{v}'\right)^{\top} \mathbf{J}^{\top} \underbrace{(\nabla_{\theta}\mathbf{u}_{\theta})(\nabla_{\theta}\mathbf{u}_{\theta})^{\top}}_{\mathbf{G}_{\theta} \succeq \mathbf{0}} \mathbf{J}\mathbf{v}' \mid \mathbf{x}_t\right] \\ &= 4 \text{Tr}(\mathbf{G}_{\theta} \mathbf{J} \Sigma_{\mathbf{v}'} \mathbf{J}^{\top}) \propto \text{Tr}(\mathbf{J} \Sigma_{\mathbf{v}'} \mathbf{J}^{\top}), \end{aligned} \quad (21)$$

where $\mathbf{G}_{\theta} = (\nabla_{\theta}\mathbf{u}_{\theta})(\nabla_{\theta}\mathbf{u}_{\theta})^{\top} \in \mathbb{R}^{d \times d}$ is the parameter-space Gram matrix and the last step uses $\mathbf{G}_{\theta} \succeq \mathbf{0}$ to establish proportionality leveraging the cyclic property of the trace. Proof completes. \square

B.3 Proof of Theorem 3 (Semi-Gradient Gap)

Theorem 3 (Semi-Gradient Gap). *The gradient of the MeanFlow loss \mathcal{L}_{MF} with and without the stop-gradient operator differ by*

$$\underbrace{2(t-r) \mathbb{E}\left[(\nabla_{\theta}(\partial_{\mathbf{x}_t}\mathbf{u}_{\theta} \cdot \mathbf{v} + \partial_t\mathbf{u}_{\theta}))^{\top} \mathbf{r}_{\theta}\right]}_{\text{mean-field gradient difference}} + \underbrace{\mathbb{E}[\nabla_{\theta} \text{Tr}(\mathbf{J} \Sigma_{\mathbf{v}'} \mathbf{J}^{\top})]}_{\text{variance-driven gradient difference}}.$$

Proof. The MeanFlow loss conditioned on \mathbf{x}_t decomposes as (cf. equation 5):

$$\mathbb{E}_{\mathbf{x}_0|\mathbf{x}_t}[\ell_{MF}] = \|\mathbf{r}_{\theta}^{\text{sg}}\|^2 + \text{Tr}(\mathbf{J} \Sigma_{\mathbf{v}'} \mathbf{J}^{\top}). \quad (22)$$

Without stop-gradient. Both terms depend on θ (through \mathbf{u}_{θ} and $\partial_{\mathbf{x}_t}\mathbf{u}_{\theta}$), so the full gradient is:

$$\nabla_{\theta}\mathbb{E}[\ell] = \nabla_{\theta}\|\mathbf{r}_{\theta}\|^2 + \nabla_{\theta}\text{Tr}(\mathbf{J} \Sigma_{\mathbf{v}'} \mathbf{J}^{\top}). \quad (23)$$

With stop-gradient. The JVP terms in $\mathbf{r}_{\theta}^{\text{sg}}$ and \mathbf{J} are treated as constants, so:

$$\nabla_{\theta}^{\text{sg}}\|\mathbf{r}_{\theta}^{\text{sg}}\|^2 = 2(\nabla_{\theta}\mathbf{u}_{\theta})^{\top} \mathbf{r}_{\theta}^{\text{sg}}, \quad \nabla_{\theta}^{\text{sg}}\text{Tr}(\mathbf{J} \Sigma_{\mathbf{v}'} \mathbf{J}^{\top}) = \mathbf{0}. \quad (24)$$

The gap between the full and stop-gradient gradients is therefore:

$$\begin{aligned} \nabla_{\theta}\mathbb{E}[\ell] - \nabla_{\theta}^{\text{sg}}\mathbb{E}[\ell] &= \underbrace{\nabla_{\theta}\|\mathbf{r}_{\theta}\|^2 - 2(\nabla_{\theta}\mathbf{u}_{\theta})^{\top} \mathbf{r}_{\theta}^{\text{sg}}}_{\text{mean-field gradient difference}} + \underbrace{\nabla_{\theta}\text{Tr}(\mathbf{J} \Sigma_{\mathbf{v}'} \mathbf{J}^{\top})}_{\text{variance-driven difference}}. \end{aligned} \quad (25)$$

Expanding the first term: $\nabla_{\theta}\|\mathbf{r}_{\theta}\|^2 = 2(\nabla_{\theta}\mathbf{r}_{\theta})^{\top} \mathbf{r}_{\theta}$, and $\nabla_{\theta}\mathbf{r}_{\theta}$ includes the derivative of the JVP terms $(t-r)(\partial_{\mathbf{x}_t}\mathbf{u}_{\theta} \cdot \mathbf{v} + \partial_t\mathbf{u}_{\theta})$ w.r.t. θ , yielding the second-order mean-field difference $2(t-r)\mathbb{E}[(\nabla_{\theta}(\partial_{\mathbf{x}_t}\mathbf{u}_{\theta} \cdot \mathbf{v} + \partial_t\mathbf{u}_{\theta}))^{\top} \mathbf{r}_{\theta}]$. At convergence $\mathbf{r}_{\theta} \rightarrow \mathbf{0}$, this term vanishes, and the gap is dominated by the variance-driven term $\nabla_{\theta}\text{Tr}(\mathbf{J} \Sigma_{\mathbf{v}'} \mathbf{J}^{\top})$. Proof completes. \square

B.4 Proof of Theorem 4 (Optimal Control-Variate Coefficient)

Theorem 4 (Optimal control-variate coefficient). *Under the scalar-isotropic approximation $\Sigma_{\mathbf{v}'} \approx \sigma^2 \mathbf{I}_d$, $\mathbf{J} \approx \kappa \mathbf{I}_d$, and the parameter-isotropy approximation $\mathbf{g}\mathbf{g}^{\top} \propto \mathbf{I}_d$,*

$$M(\beta) \propto \beta^2(\kappa+1)^2 \|\mathbf{b}\|^2 + \sigma^2 d((1-\beta)\kappa - \beta)^2.$$

For $\kappa > 0$, $M(\beta)$ admits a unique minimizer

$$\beta^* = \underbrace{\frac{\kappa}{\kappa+1}}_{\text{noise-cancellation}} \cdot \underbrace{\frac{\sigma^2 d}{\sigma^2 d + \|\mathbf{b}\|^2}}_{\text{shrinkage}},$$

with optimum value $M(\beta^*) \propto \sigma^2 d \kappa^2 \|\mathbf{b}\|^2 / (\sigma^2 d + \|\mathbf{b}\|^2)$.

Proof. From equation 9, we can decompose gradient with coefficient β into:

$$\mathbf{g}^{(\beta)} = 2\mathbf{g}^\top \left[\mathbf{r}_\theta + ((1-\beta)\mathbf{J} - \beta\mathbf{I})\mathbf{v}' + \beta(\mathbf{J}+\mathbf{I})\mathbf{b} \right]. \quad (26)$$

Leveraging the property $\mathbb{E}_{\mathbf{x}_0|\mathbf{x}_t}[\mathbf{v}'] = \mathbf{0}$, the conditional mean is $\mathbb{E}[\mathbf{g}^{(\beta)} | \mathbf{x}_t] = 2\mathbf{g}^\top (\mathbf{r}_\theta + \beta(\mathbf{J}+\mathbf{I})\mathbf{b})$ and the centered noise is $-2\mathbf{g}^\top ((1-\beta)\mathbf{J} - \beta\mathbf{I})\mathbf{v}'$ (relative to the ideal target $2\mathbf{g}^\top \mathbf{r}_\theta$). The conditional MSE w.r.t. the ideal target therefore decomposes as

$$\text{MSE} = \underbrace{4\beta^2 \|\mathbf{g}^\top (\mathbf{J}+\mathbf{I})\mathbf{b}\|^2}_{\text{bias}^2} + \underbrace{4 \text{Tr}(\mathbf{g}\mathbf{g}^\top ((1-\beta)\mathbf{J} - \beta\mathbf{I})\Sigma_{\mathbf{v}'}((1-\beta)\mathbf{J} - \beta\mathbf{I})^\top)}_{\text{variance}}. \quad (27)$$

We then solve for the MSE and prove its strict convexity. Let $\mathbf{A} \triangleq \mathbf{J}+\mathbf{I}$ and $\mathbf{G}_\theta \triangleq \mathbf{g}\mathbf{g}^\top \succeq \mathbf{0}$. Substituting $((1-\beta)\mathbf{J} - \beta\mathbf{I}) = \mathbf{J} - \beta\mathbf{A}$ and using $\|\mathbf{g}^\top \mathbf{A}\mathbf{b}\|^2 = \text{Tr}(\mathbf{G}_\theta \mathbf{A}\mathbf{b}\mathbf{b}^\top \mathbf{A}^\top)$, the conditional MSE writes as a quadratic in β :

$$M(\beta) = \alpha_0 - 2\alpha_1\beta + \alpha_2\beta^2, \quad (28)$$

with

$$\begin{aligned} \alpha_0 &\triangleq \text{Tr}(\mathbf{G}_\theta \mathbf{J} \Sigma_{\mathbf{v}'} \mathbf{J}^\top), \\ \alpha_1 &\triangleq \text{Tr}(\mathbf{G}_\theta \mathbf{J} \Sigma_{\mathbf{v}'} \mathbf{A}^\top), \\ \alpha_2 &\triangleq \text{Tr}(\mathbf{G}_\theta \mathbf{A} (\Sigma_{\mathbf{v}'} + \mathbf{b}\mathbf{b}^\top) \mathbf{A}^\top). \end{aligned}$$

We exploit the symmetry of \mathbf{G}_θ and $\Sigma_{\mathbf{v}'}$ to consolidate the linear-in- β trace into a single α_1 . The Hessian is then positive:

$$\frac{\partial^2}{\partial \beta^2} M(\beta) = 2\alpha_2 = 2 \text{Tr}(\mathbf{G}_\theta \mathbf{A} (\Sigma_{\mathbf{v}'} + \mathbf{b}\mathbf{b}^\top) \mathbf{A}^\top) \geq 0, \quad (29)$$

since each factor inside the trace is positive semi-definite (*i.e.*, $\mathbf{G}_\theta \succeq \mathbf{0}$, $\Sigma_{\mathbf{v}'} + \mathbf{b}\mathbf{b}^\top \succeq \mathbf{0}$, and $\mathbf{A}(\Sigma_{\mathbf{v}'} + \mathbf{b}\mathbf{b}^\top) \mathbf{A}^\top = \mathbf{M}\mathbf{M}^\top \succeq \mathbf{0}$ for $\mathbf{M} \triangleq \mathbf{A}(\Sigma_{\mathbf{v}'} + \mathbf{b}\mathbf{b}^\top)^{1/2}$). Therefore, $M(\beta)$ is convex in β . However, the Hessian is strictly positive iff $\mathbf{G}_\theta^{1/2} \mathbf{M} \neq \mathbf{0}$, which holds outside two pathological regimes: (i) $\mathbf{A} = \mathbf{0}$, or equivalently $\mathbf{J} = -\mathbf{I}$, in which case the linear coefficient α_1 also vanishes and $M(\beta)$ is constant; (ii) $\mathbf{g} = \mathbf{0}$ (*e.g.*, *frozen parameters*). Otherwise, $M(\beta)$ is *strictly* convex with unique unconstrained minimizer

$$\beta_{\text{matrix}}^* = \frac{\alpha_1}{\alpha_2} = \frac{\text{Tr}(\mathbf{G}_\theta \mathbf{J} \Sigma_{\mathbf{v}'} (\mathbf{J}+\mathbf{I})^\top)}{\text{Tr}(\mathbf{G}_\theta (\mathbf{J}+\mathbf{I})(\Sigma_{\mathbf{v}'} + \mathbf{b}\mathbf{b}^\top)(\mathbf{J}+\mathbf{I})^\top)}. \quad (30)$$

Note that β_{matrix}^* may fall outside $[0, 1]$; the box-constrained optimum on the $\beta \in [0, 1]$ interval (cf. equation 8) is then $\text{clip}(\beta_{\text{matrix}}^*, 0, 1)$, attained at the nearer endpoint by convexity.

Finally, we derive the scalar approximation. Substituting $\mathbf{J} = \kappa\mathbf{I}_d$, $\Sigma_{\mathbf{v}'} = \sigma^2\mathbf{I}_d$, $\mathbf{A} = (\kappa+1)\mathbf{I}_d$, and the parameter-isotropy approximation $\mathbf{G}_\theta \propto \mathbf{I}_d$ yields

$$\alpha_0 \propto \sigma^2\kappa^2d, \quad \alpha_1 \propto \sigma^2\kappa(\kappa+1)d, \quad \alpha_2 \propto (\kappa+1)^2(\sigma^2d + \|\mathbf{b}\|^2),$$

which equivalently gives

$$M(\beta) \propto \beta^2(\kappa+1)^2\|\mathbf{b}\|^2 + \sigma^2d((1-\beta)\kappa - \beta)^2. \quad (31)$$

Taking the derivative with respect to β and setting it to zero gives:

$$\beta^* = \frac{\alpha_1}{\alpha_2} = \frac{\sigma^2\kappa(\kappa+1)d}{(\kappa+1)^2(\sigma^2d + \|\mathbf{b}\|^2)} = \frac{\kappa}{\kappa+1} \cdot \frac{\sigma^2d}{\sigma^2d + \|\mathbf{b}\|^2}. \quad (32)$$

At β^* above, we have $(1-\beta^*)\kappa - \beta^* = \kappa\|\mathbf{b}\|^2/(\sigma^2d + \|\mathbf{b}\|^2)$. Substituting it back recovers:

$$M(\beta^*) \propto \frac{\sigma^2d\kappa^2\|\mathbf{b}\|^2}{\sigma^2d + \|\mathbf{b}\|^2}.$$

For $\kappa > 0$ and $\|\mathbf{b}\|^2 > 0$: $M(\beta^*)/M(0) = \|\mathbf{b}\|^2/(\sigma^2d + \|\mathbf{b}\|^2) < 1$, so $M(\beta^*) < M(0)$. For the $M(1)$ comparison, $M(1) - M(\beta^*) \propto (\kappa+1)^2\|\mathbf{b}\|^2 + \sigma^2d - \sigma^2d\kappa^2\|\mathbf{b}\|^2/(\sigma^2d + \|\mathbf{b}\|^2)$, and the first two terms exceed $\sigma^2d\kappa^2\|\mathbf{b}\|^2/(\sigma^2d + \|\mathbf{b}\|^2)$ since $(\kappa+1)^2 > \kappa^2$ for $\kappa > 0$. Strict dominance is therefore over the unconstrained interior optimum; if $\beta_{\text{matrix}}^* \notin [0, 1]$, the box-constrained optimum is at the nearer corner, and the dominance is non-strict. \square

B.5 Proof of Proposition 1 (Gradient under the $\beta = 1$ corner loss)

Proposition 1 (Gradient under the $\beta = 1$ corner loss). *The gradient of \mathcal{L}_{MF}^{EMA} takes the form*

$$\nabla_{\theta} \mathcal{L}_{MF}^{EMA} = 2 \mathbb{E}[\mathbf{g} \tilde{\mathbf{r}}^{EMA}],$$

where $(\nabla_{\theta} \mathbf{u}_{\theta}) \in \mathbb{R}^{d \times p}$ is the parameter Jacobian, $\tilde{\mathbf{r}}^{EMA} \triangleq V_{\theta}^{EMA} - \mathbf{v}(\mathbf{x}_t, t) \in \mathbb{R}^d$, and no $\mathbf{J}\mathbf{v}'$ noise term appears.

Proof. The EMA velocity anchor $\mathbf{u}_{\bar{\theta}}(\mathbf{x}_t, t, t)$ is deterministic given \mathbf{x}_t , since the EMA parameters $\bar{\theta}$ are fixed during the gradient step. Under stop-gradient, V_{θ}^{EMA} depends on θ only through $\mathbf{u}_{\theta}(\mathbf{x}_t, r, t)$. By the same argument as equation 19, the per-step gradient is:

$$\nabla_{\theta} \ell = 2 (\nabla_{\theta} \mathbf{u}_{\theta})^{\top} (V_{\theta}^{EMA} - \mathbf{v}_{\text{cond}}). \quad (33)$$

Writing $\mathbf{v}_{\text{cond}} = \mathbf{v}(\mathbf{x}_t, t) + \mathbf{v}'$ and noting that $\tilde{\mathbf{r}}^{EMA} := V_{\theta}^{EMA} - \mathbf{v}(\mathbf{x}_t, t)$ is deterministic given \mathbf{x}_t :

$$\mathbb{E}_{\mathbf{x}_0 | \mathbf{x}_t} [\nabla_{\theta} \ell] = 2 (\nabla_{\theta} \mathbf{u}_{\theta})^{\top} \tilde{\mathbf{r}}^{EMA}, \quad (34)$$

since $\mathbb{E}[\mathbf{v}' | \mathbf{x}_t] = \mathbf{0}$. The tower property $\nabla_{\theta} \mathcal{L}_{MF}^{EMA} = \mathbb{E}_{r, t, \mathbf{x}_t} [\mathbb{E}_{\mathbf{x}_0 | \mathbf{x}_t} [\nabla_{\theta} \ell]]$ gives the stated result. Crucially, no $\mathbf{J}\mathbf{v}'$ term appears because the EMA tangent is deterministic; compare with the original MeanFlow gradient equation 19 where the stochastic tangent produces the $\mathbf{J}\mathbf{v}'$ noise. \square

B.6 Proof of Proposition 2 (Bias-Variance Tradeoff)

Proposition 2 (Bias-Variance Tradeoff). *The EMA mean-field residual decomposes as*

$$\tilde{\mathbf{r}}^{EMA} = \mathbf{r}_{\theta} + (t-r) \partial_{\mathbf{x}_t} \mathbf{u}_{\theta} (\mathbf{u}_{\bar{\theta}}(\mathbf{x}_t, t, t) - \mathbf{v}(\mathbf{x}_t, t)),$$

where \mathbf{r}_{θ} is the true MeanFlow residual. The FM anchor drives $\mathbf{u}_{\bar{\theta}}(\mathbf{x}_t, t, t) \rightarrow \mathbf{v}(\mathbf{x}_t, t)$, giving $\tilde{\mathbf{r}}^{EMA} \rightarrow \mathbf{0}$.

Proof. Expanding V_{θ}^{EMA} from equation 38, the value of the compound prediction (ignoring the stop-gradient, which does not affect values) is:

$$V_{\theta}^{EMA} = \mathbf{u}_{\theta} + (t-r) (\partial_{\mathbf{x}_t} \mathbf{u}_{\theta} \cdot \mathbf{u}_{\bar{\theta}}(\mathbf{x}_t, t, t) + \partial_t \mathbf{u}_{\theta}). \quad (35)$$

The true MeanFlow residual (with the marginal velocity as tangent) is:

$$\mathbf{r}_{\theta} = \mathbf{u}_{\theta} + (t-r) (\partial_{\mathbf{x}_t} \mathbf{u}_{\theta} \cdot \mathbf{v}(\mathbf{x}_t, t) + \partial_t \mathbf{u}_{\theta}) - \mathbf{v}(\mathbf{x}_t, t). \quad (36)$$

Subtracting:

$$\begin{aligned} \tilde{\mathbf{r}}^{EMA} &= V_{\theta}^{EMA} - \mathbf{v}(\mathbf{x}_t, t) \\ &= \mathbf{r}_{\theta} + (t-r) \partial_{\mathbf{x}_t} \mathbf{u}_{\theta} (\mathbf{u}_{\bar{\theta}}(\mathbf{x}_t, t, t) - \mathbf{v}(\mathbf{x}_t, t)). \end{aligned} \quad (37)$$

At convergence, the true residual $\mathbf{r}_{\theta} \rightarrow \mathbf{0}$ (the MeanFlow identity is satisfied) and the FM anchor loss equation 39 supervises the boundary condition, driving $\mathbf{u}_{\bar{\theta}}(\mathbf{x}_t, t, t) \rightarrow \mathbf{v}(\mathbf{x}_t, t)$ and hence $\tilde{\mathbf{r}}^{EMA} \rightarrow \mathbf{0}$. \square

B.7 Proof of Proposition 3 (Target/Tangent Bias Asymmetry)

Proposition 3 (Target/Tangent Bias Asymmetry). *Let $\hat{\mathbf{v}} = \mathbf{u}_{\bar{\theta}}(\mathbf{x}_t, t, t)$ be a deterministic proxy with bias $\mathbf{b} \triangleq \hat{\mathbf{v}} - \mathbf{v}(\mathbf{x}_t, t)$. Consider two ways of substituting $\hat{\mathbf{v}}$ into equation 4:*

- (i) Tangent replacement (the $\beta = 1$ corner): *keep the target \mathbf{v}_{cond} but replace the JVP tangent. At the loss minimum,*

$$\mathbf{u}^*(\mathbf{x}_t, r, t) - \mathbf{v}(\mathbf{x}_t, t) = -\frac{1}{2}(t-r) \partial_{\mathbf{x}_t} \mathbf{u}^* \mathbf{b} + \mathcal{O}((t-r) \|\mathbf{b}\|^2),$$

so the stationary error is $\mathcal{O}((t-r) \|\partial_{\mathbf{x}_t} \mathbf{u}\| \|\mathbf{b}\|)$ and vanishes at $r \rightarrow t$.

- (ii) Target replacement: substitute \hat{v} for \mathbf{v}_{cond} in the regression target. At $r=t$ the loss minimum satisfies

$$\mathbf{u}^*(\mathbf{x}_t, t, t) - \mathbf{v}(\mathbf{x}_t, t) = \mathbf{b},$$

i.e., the stationary error equals the proxy bias exactly, uniformly in t and independent of the gap $(t-r)$.

Proof. Tangent replacement. Substituting \hat{v} for \mathbf{v}_{cond} only in the JVP tangent (target unchanged) gives the per-sample compound prediction

$$V_{\theta}^{\text{EMA}} = \mathbf{u}_{\theta} + (t-r)(\partial_{\mathbf{x}_t} \mathbf{u}_{\theta} \cdot \hat{v} + \partial_t \mathbf{u}_{\theta}),$$

and the loss is $\mathbb{E} \|V_{\theta}^{\text{EMA}} - \mathbf{v}_{\text{cond}}\|^2$. By stationarity, $\mathbb{E}[V_{\theta}^{\text{EMA}} - \mathbf{v}_{\text{cond}} | \mathbf{x}_t] = \mathbf{0}$ at the minimum. Taking conditional expectation and using $\mathbb{E}[\mathbf{v}_{\text{cond}} | \mathbf{x}_t] = \mathbf{v}(\mathbf{x}_t, t)$,

$$\mathbf{u}^* + (t-r)(\partial_{\mathbf{x}_t} \mathbf{u}^* \cdot \hat{v} + \partial_t \mathbf{u}^*) = \mathbf{v}(\mathbf{x}_t, t).$$

At the same point, the *true* MeanFlow identity (with the marginal velocity as tangent) reads

$$\mathbf{u}^{\diamond} + (t-r)(\partial_{\mathbf{x}_t} \mathbf{u}^{\diamond} \cdot \mathbf{v} + \partial_t \mathbf{u}^{\diamond}) = \mathbf{v}(\mathbf{x}_t, t),$$

with $\mathbf{u}^{\diamond}(\mathbf{x}_t, t, t) = \mathbf{v}(\mathbf{x}_t, t)$. Subtracting and writing $\mathbf{u}^* = \mathbf{u}^{\diamond} + \Delta$,

$$\Delta + (t-r) \partial_{\mathbf{x}_t} \mathbf{u}^* \mathbf{b} + (t-r) D_t \Delta = \mathbf{0}, \quad D_t \Delta \triangleq \partial_t \Delta + \mathbf{v} \cdot \partial_{\mathbf{x}_t} \Delta,$$

with the boundary condition $\Delta(\mathbf{x}_t, t, t) = \mathbf{0}$. Substituting $s = t-r$ at fixed r converts this to a first-order linear ODE in s :

$$s \frac{d\Delta}{ds} + \Delta = -s \partial_{\mathbf{x}_t} \mathbf{u}^* \mathbf{b} + \mathcal{O}(\|\mathbf{b}\|^2),$$

which has $s\Delta(s) = -\frac{s^2}{2} \partial_{\mathbf{x}_t} \mathbf{u}^* \mathbf{b} + C$; the boundary condition $\Delta(0) = \mathbf{0}$ forces $C = 0$. Hence

$$\Delta(\mathbf{x}_t, r, t) = -\frac{1}{2}(t-r) \partial_{\mathbf{x}_t} \mathbf{u}^* \mathbf{b} + \mathcal{O}((t-r) \|\mathbf{b}\|^2),$$

i.e., the stationary error is $\mathcal{O}((t-r) \|\partial_{\mathbf{x}_t} \mathbf{u}\| \|\mathbf{b}\|)$ and vanishes at the boundary $r \rightarrow t$. The factor of $\frac{1}{2}$ comes from integrating the material-derivative term, which contributes equally to the leading-order coefficient as the bias source term.

Target replacement. Substituting \hat{v} for \mathbf{v}_{cond} in the regression target yields the loss $\mathbb{E} \|\mathbf{u}_{\theta} + (t-r) D\mathbf{u}/Dt - \hat{v}\|^2$. By stationarity, the loss minimum satisfies $\mathbb{E}[\mathbf{u}^* + (t-r) D\mathbf{u}^*/Dt - \hat{v} | \mathbf{x}_t] = \mathbf{0}$. Specializing to $r=t$, the gap term vanishes and the equation collapses to $\mathbf{u}^*(\mathbf{x}_t, t, t) = \hat{v} = \mathbf{v}(\mathbf{x}_t, t) + \mathbf{b}$, so the stationary error at the boundary is exactly \mathbf{b} , independent of (t, r) .

Asymmetry. Tangent replacement carries a multiplicative $(t-r)$ factor on the bias and is therefore pinned to zero at the boundary $r=t$ that the FM anchor enforces; target replacement carries no such factor, and the bias persists at every t , requiring a boundary regularizer at *every* (r, t) to remove. \square

C Implementation Details

To validate the framework empirically in section 5, we instantiate the $\beta = 1$ corner of theorem 4 through two design choices at near-zero compute overhead:

EMA proxy. We take $\hat{v} = \mathbf{u}_{\bar{\theta}}(\mathbf{x}_t, t, t)$ where $\bar{\theta}$ is a Polyak-averaged [4, 5] (a.k.a. *exponential moving-average*) copy of θ , where $\bar{\theta} \leftarrow \mu \bar{\theta} + (1-\mu)\theta$ with $\mu \in [0, 1)$. The resulting loss replaces the conditional tangent in equation 4 with the EMA proxy:

$$\mathcal{L}_{\text{MF}}^{\text{EMA}}(\theta) = \mathbb{E}_{r,t,\mathbf{x}_0,\mathbf{x}_1} \left[\|\mathbf{u}_{\theta} + (t-r) \text{sg}[\text{JVP}(\mathbf{u}_{\theta}, (\mathbf{x}_t, r, t), (\mathbf{u}_{\bar{\theta},t}, 0, 1))] - \mathbf{v}_{\text{cond}}\|_2^2 \right], \quad (38)$$

with $\mathbf{u}_{\bar{\theta},t} \triangleq \mathbf{u}(\mathbf{x}_t, t, t; \bar{\theta})$. Crucially, the regression target remains \mathbf{v}_{cond} : the tangent and target play distinct statistical roles per section 3.1, and we only need to replace the tangent.

Flow-matching anchor. The proxy bias $\mathbf{b} = \mathbf{u}_{\bar{\theta},t} - \mathbf{v}$ must be controlled or it propagates through the $\beta(\mathbf{J}+\mathbf{I})\mathbf{b}$ bias term. We supervise the boundary condition $\mathbf{u}(\mathbf{x}_t, t, t) = \mathbf{v}(\mathbf{x}_t, t)$ directly with a small flow-matching loss

$$\mathcal{L}_{\text{FM}}(\theta) = \mathbb{E}_{t,\mathbf{x}_0,\mathbf{x}_1} \left[\|\mathbf{u}_{\theta}(\mathbf{x}_t, t-\delta, t) - \mathbf{v}_{\text{cond}}\|_2^2 \right], \quad (39)$$

Algorithm 1 Training the $\beta=1$ instantiation with EMA tangent and FM anchor loss

Require: Dataset \mathcal{D} , EMA decay μ , anchor weight λ , anchor interval $[\delta_{\min}, \delta_{\max}]$, learning rate η

Initialize $\hat{\theta} \leftarrow \theta$

for $k = 1, 2, \dots$ **do**

Sample $(\mathbf{x}_0, \mathbf{x}_1) \sim \mathcal{D} \times \mathcal{N}(\mathbf{0}, \mathbf{I}_d)$, $t \sim \mathcal{U}[0, 1]$, $r \sim \mathcal{U}[0, t]$, $\delta \sim \mathcal{U}[\delta_{\min}, \delta_{\max}]$

$\mathbf{x}_t \leftarrow (1-t)\mathbf{x}_0 + t\mathbf{x}_1$, $\mathbf{v}_{\text{cond}} \leftarrow \mathbf{x}_1 - \mathbf{x}_0$

$\mathbf{v}_{\text{tang}} \leftarrow \text{sg}[\mathbf{u}_{\hat{\theta}}(\mathbf{x}_t, t, t)]$ ▷ EMA tangent (one extra forward pass)

$V_{\hat{\theta}} \leftarrow \mathbf{u}_{\hat{\theta}}(\mathbf{x}_t, r, t) + (t-r) \text{sg}[\text{JVP}(\mathbf{u}_{\hat{\theta}}, (\mathbf{x}_t, r, t), (\mathbf{v}_{\text{tang}}, 0, 1))]$

$\ell_{\text{MF}} \leftarrow \|V_{\hat{\theta}} - \mathbf{v}_{\text{cond}}\|_2^2$

$\ell_{\text{FM}} \leftarrow \|\mathbf{u}_{\hat{\theta}}(\mathbf{x}_t, t-\delta, t) - \mathbf{v}_{\text{cond}}\|_2^2$ ▷ FM anchor (one extra forward pass)

$\theta \leftarrow \theta - \eta \nabla_{\theta}(\ell_{\text{MF}} + \lambda \ell_{\text{FM}})$

$\hat{\theta} \leftarrow \mu \hat{\theta} + (1-\mu)\theta$ ▷ EMA update

end for

return $\hat{\theta}$ ▷ Generate: $\hat{\mathbf{x}}_0 = \mathbf{x}_1 - \mathbf{u}_{\hat{\theta}}(\mathbf{x}_1, 0, 1)$

where $\delta \sim \mathcal{U}[\delta_{\min}, \delta_{\max}]$ with $\delta_{\max} \ll 1$. Here, we evaluate the anchor at a small *interior* time offset rather than at the boundary $\delta=0$ for two reasons. First, the same $\mathbf{u}(\mathbf{x}_t, t-\delta, t)$ is what the EMA tangent eventually converges to, so the anchor and the JVP target share the same network-evaluation pattern. Meanwhile, we found training to be slightly more stable when the anchor probes a thin neighborhood of the boundary rather than a single $r=t$ slice. For small δ , $\mathbf{u}(\mathbf{x}_t, t-\delta, t)$ approximates the instantaneous velocity, and equation 1 guarantees $\mathbb{E}[\mathbf{v}_{\text{cond}} | \mathbf{x}_t] = \mathbf{v}(\mathbf{x}_t, t)$, so \mathcal{L}_{FM} drives $\mathbf{u}_{\hat{\theta}}(\mathbf{x}_t, t, t) \rightarrow \mathbf{v}(\mathbf{x}_t, t)$, and via EMA, $\mathbf{u}_{\hat{\theta}}(\mathbf{x}_t, t, t) \rightarrow \mathbf{v}$ and hence $\mathbf{b} \rightarrow \mathbf{0}$. The full $\beta=1$ corner loss is

$$\mathcal{L}_{\beta=1}(\theta) = \mathcal{L}_{\text{MF}}^{\text{EMA}}(\theta) + \lambda \mathcal{L}_{\text{FM}}(\theta), \quad (40)$$

with $\lambda > 0$. The training procedure is algorithm 1. For the hyperparameters in our experiments, we use $(\delta_{\min}, \delta_{\max}, \lambda) = (10^{-4}, 10^{-2}, 0.5)$ for 2-D toy and DGMM runs, and $(\delta_{\min}, \delta_{\max}, \lambda) = (0, 10^{-3}, 0.1)$ for training the DiT-B/4 on ImageNet-256 with $\beta=1$.

Optimality. The combination of EMA proxy plus FM anchor approximates the $\beta \rightarrow 1$ limit of theorem 4 at the cost of one additional JVP per step. Propositions 1 to 3 (stated and proved in appendix B) characterize the recipe theoretically: the $\mathbf{J}\mathbf{v}'$ amplification of theorem 2 is eliminated under the EMA tangent (Proposition 1); the residual EMA bias is controlled by the FM anchor (Proposition 2); and a target/tangent asymmetry justifies why the FM anchor at the boundary $r=t$ alone is sufficient since the tangent-replacement bias is multiplicatively damped by $(t-r)$, while target-replacement bias is not (Proposition 3). The same asymmetry locates a failure mode of self-distillation-style variants that use a deterministic proxy for both roles, where the trivial fixed point $\mathbf{u}^* \equiv \hat{\mathbf{v}}$ persists without continual external supervision [6, 7].

D Additional Results

D.1 2-D Toy Benchmark

Table 4 reports the matched-method comparison of the original MeanFlow ($\beta=0$) against the full $\beta=1$ corner recipe (EMA tangent + FM anchor; hyperparameters in appendix C, no trace weight, no adaptive weighting) on six 2-D datasets, averaged over three seeds at 200k optimization steps. The $\beta=1$ recipe reduces SW_1 on five of six datasets, with the largest reduction (54%) on `swiss_roll`. `two_spirals` is a known low-curvature outlier where the original MeanFlow already attains the lowest absolute SW_1 ; the empirical $\beta^*=0$ on the β -sweep agrees.

D.2 Full β -sweep grid on DGMM

Table 5 reports SW_1 at convergence for every (d, β) pair, with mean \pm SEM over three seeds. The bolded cell per row is the empirical $\beta^* = \arg \min_{\beta} \text{SW}_1(\beta)$; the summary view in table 2 (main text) compares only $\beta=0$ and β^* per dimension. The grid makes the β -insensitivity of low- d rows visible at full precision: SW_1 is uniform to three decimal places for $d \in \{4, 8, 16\}$.

Table 4: Sliced Wasserstein distance (lower is better) on the 2-D toy benchmark, averaged over three seeds $\{42, 0, 1\}$ at 200k steps. SW_p is evaluated on 4096 samples with 500 random projections; both metrics use the *same* projection key per evaluation for variance-reduced paired estimates.

| Dataset | Metric | MeanFlow ($\beta=0$) | $\beta=1$ |
|-----------------|--------|-------------------------------------|-------------------------------------|
| checkerboard | SW_1 | 0.175 ± 0.036 | 0.134 ± 0.029 |
| | SW_2 | 0.234 ± 0.042 | 0.175 ± 0.046 |
| eight_gaussians | SW_1 | 0.098 ± 0.016 | 0.085 ± 0.010 |
| | SW_2 | 0.151 ± 0.022 | 0.146 ± 0.023 |
| two_moons | SW_1 | 0.093 ± 0.028 | 0.072 ± 0.019 |
| | SW_2 | 0.177 ± 0.068 | 0.093 ± 0.025 |
| swiss_roll | SW_1 | 0.098 ± 0.058 | 0.045 ± 0.003 |
| | SW_2 | 0.177 ± 0.151 | 0.060 ± 0.007 |
| two_spirals | SW_1 | 0.034 ± 0.001 | 0.037 ± 0.001 |
| | SW_2 | 0.044 ± 0.001 | 0.046 ± 0.001 |
| pinwheel | SW_1 | 0.094 ± 0.011 | 0.059 ± 0.005 |
| | SW_2 | 0.128 ± 0.014 | 0.076 ± 0.005 |

Table 5: DGMM β -sweep: full grid of mean \pm SEM SW_1 at convergence (200k steps, three seeds $\{42, 0, 1\}$). Bolded cell per column marks the empirical $\beta^* = \arg \min_{\beta} SW_1(\beta)$ at that dimension. The summary view is in Table 2.

| β | d | | | | | |
|---------|-------------------------------------|-------------------------------------|-------------------------------------|-------------------------------------|-------------------------------------|-------------------------------------|
| | 2 | 4 | 8 | 16 | 32 | 64 |
| 0.0 | 0.152 ± 0.022 | 0.083 ± 0.011 | 0.062 ± 0.003 | 0.044 ± 0.002 | 0.034 ± 0.001 | 0.028 ± 0.003 |
| 0.1 | 0.151 ± 0.025 | 0.083 ± 0.011 | 0.062 ± 0.003 | 0.044 ± 0.002 | 0.034 ± 0.001 | 0.027 ± 0.003 |
| 0.2 | 0.149 ± 0.024 | 0.083 ± 0.011 | 0.062 ± 0.003 | 0.044 ± 0.002 | 0.037 ± 0.003 | 0.028 ± 0.003 |
| 0.3 | 0.148 ± 0.022 | 0.083 ± 0.011 | 0.062 ± 0.003 | 0.044 ± 0.002 | 0.038 ± 0.004 | 0.028 ± 0.003 |
| 0.4 | 0.149 ± 0.022 | 0.083 ± 0.011 | 0.062 ± 0.003 | 0.044 ± 0.002 | 0.041 ± 0.007 | 0.025 ± 0.000 |
| 0.5 | 0.150 ± 0.022 | 0.084 ± 0.011 | 0.062 ± 0.003 | 0.044 ± 0.002 | 0.041 ± 0.007 | 0.026 ± 0.001 |
| 0.6 | 0.150 ± 0.021 | 0.083 ± 0.011 | 0.062 ± 0.003 | 0.044 ± 0.002 | 0.035 ± 0.001 | 0.026 ± 0.001 |
| 0.7 | 0.148 ± 0.020 | 0.083 ± 0.011 | 0.062 ± 0.003 | 0.044 ± 0.002 | 0.034 ± 0.001 | 0.026 ± 0.001 |
| 0.8 | 0.148 ± 0.016 | 0.083 ± 0.011 | 0.062 ± 0.003 | 0.044 ± 0.002 | 0.036 ± 0.002 | 0.027 ± 0.002 |
| 0.9 | 0.148 ± 0.015 | 0.083 ± 0.011 | 0.062 ± 0.003 | 0.044 ± 0.002 | 0.037 ± 0.003 | 0.027 ± 0.001 |
| 1.0 | 0.146 ± 0.015 | 0.083 ± 0.011 | 0.062 ± 0.003 | 0.044 ± 0.003 | 0.036 ± 0.002 | 0.028 ± 0.001 |

D.3 Latent DiT-B/4 on ImageNet-256

We test whether the variance-reduction mechanism of theorems 2 and 4 scales beyond toys by training DiT [8] variants on ImageNet in the latent space of a frozen Stable Diffusion VAE, following the recipe of [9]. The four β configurations share identical hyperparameters and code paths; only the loss differs (*i.e.*, the original MeanFlow MSE for the interior β runs versus the EMA-tangent loss in equation 40 for the $\beta=1$ corner).

Setup. Logit-normal (r, t) sampling with mean -0.4 and stddev 1, overlap rate 0.75, AdamW with constant learning rate 10^{-4} , EMA decay 0.9999, batch size 256 across 32 TPU v4 chips. All four configurations ($\beta \in \{0, 0.25, 0.5, 1\}$) share the same DiT-B/4 backbone, data pipeline, optimizer, EMA schedule, and (r, t) sampling distribution. The interior β runs ($\beta \in \{0, 0.25, 0.5\}$) reuse the baseline configuration verbatim and add only the tangent-mixing rule of equation 8; the $\beta=1$ corner additionally turns off the Karras-style adaptive loss weighting and adds the FM anchor of equation 39 (DiT anchor hyperparameters in appendix C). The extra EMA forward pass and FM-anchor evaluation per step add up to a $\sim 22\%$ wall-clock overhead on TPU v4 (2.20 steps/s for $\beta=1$ versus 2.65 steps/s for the baseline); the $\beta \in \{0.25, 0.5\}$ interior runs incur only the EMA forward overhead ($\sim 10\%$).

Table 6: DiT-B/4 / ImageNet-256 FID_{50k} (lower is better) at representative 5k-step checkpoints across the four-point β -sweep. All four runs completed their scheduled 300k-step training and have a matched-step eval at step 295k. Bottom rows give the matched-step deltas. The four-point ordering $\text{FID}(\beta=0) < \text{FID}(\beta=0.25) < \text{FID}(\beta=0.5) < \text{FID}(\beta=1)$ holds at every 5k-aligned matched-step checkpoint after the early-training transient (54 consecutive datapoints from step 30k to step 295k).

| step (k) | 30 | 50 | 100 | 150 | 200 | 250 | 275 | 295 |
|-------------------------------------|-------|-------|-------|-------|-------|-------|-------|---------------|
| baseline ($\beta=0$) | 128.9 | 54.5 | 22.0 | 15.5 | 13.0 | 11.9 | 11.6 | 11.37 |
| $\beta=0.25$ | 138.5 | 61.6 | 23.3 | 16.2 | 13.3 | 12.1 | 11.7 | 11.76 |
| $\beta=0.5$ | 145.2 | 66.9 | 25.6 | 17.6 | 14.4 | 13.2 | 12.7 | 12.51 |
| $\beta=1$ | 148.8 | 79.9 | 41.7 | 32.1 | 27.6 | 25.1 | 24.1 | 23.36 |
| Δ ($\beta=0.25$ – baseline) | +9.5 | +7.1 | +1.3 | +0.7 | +0.4 | +0.2 | +0.1 | +0.39 |
| Δ ($\beta=0.5$ – baseline) | +16.2 | +12.4 | +3.6 | +2.1 | +1.4 | +1.3 | +1.0 | +1.14 |
| Δ ($\beta=1$ – baseline) | +19.9 | +25.4 | +19.7 | +16.6 | +14.6 | +13.2 | +12.5 | +11.99 |

Four-point matched-step ordering. Table 6 reports FID_{50k} at representative 5k-step checkpoints for all four runs. After the early-training transient ($\leq 25k$ steps), the empirical four-point ordering $\text{FID}(\beta=0) < \text{FID}(\beta=0.25) < \text{FID}(\beta=0.5) < \text{FID}(\beta=1)$ holds at *every* 5k-aligned matched-step checkpoint we logged (54 consecutive datapoints from step 30k to step 295k). The $\beta=0.25$ vs baseline gap stays positive throughout, ranging from +9.5 early in training (step 30k) to a tight +0.39 at step 295k. The $\beta=0.5$ vs baseline gap stabilizes around +1.0 \sim +1.5 in the converged regime (steps 200k to 295k), and the $\beta=1$ vs baseline gap remains +12 \sim +14 across the converged regime.

Converged FID floors and four-point ordering. All four configurations completed their scheduled 300k-step training and have a matched-step eval at step 295k. The four FID floors at step 295k recover the bias-variance ordering of theorem 4:

$$\begin{aligned}
 \text{FID}(\beta=0) &= 11.37 \\
 \text{FID}(\beta=0.25) &= 11.76 \\
 \text{FID}(\beta=0.5) &= 12.51 \\
 \text{FID}(\beta=1) &= 23.36 \\
 \text{FID}(\beta=0) &< \text{FID}(\beta=0.25) < \text{FID}(\beta=0.5) < \text{FID}(\beta=1)
 \end{aligned}$$

Quantitatively, taking offsets from the baseline floor 11.37, $\Delta\text{FID}(\beta=0.5) \approx 1.14$ and $\Delta\text{FID}(\beta=1) \approx 11.99$. Anchoring the gradient-MSE prediction $\beta^2 \cdot A$ at the $\beta=0.5$ point gives $A \approx 4.58$, so the predicted offset at $\beta=1$ is 4.58 — the empirical 11.99 exceeds this by $\sim 2.6\times$. The FID landscape is therefore *super-linear* in the MSE-axis bias: it penalizes large bias more aggressively than gradient MSE does, which pulls the FID-optimal β past the gradient-MSE interior minimizer to the unbiased corner $\beta=0$. The four-point ordering is the strongest empirical confirmation of the bias-variance decomposition we obtain at the DiT scale.

Bias and shrinkage trajectory. To localize the predicted optimum we measure two diagnostics on the DiT checkpoints: an EMA-tracking proxy $\|\widehat{\mathbf{b}}\|^2 \triangleq \mathbb{E}_{\mathbf{x}_t} [\|\mathbf{u}_\theta(\mathbf{x}_t, t, t) - \mathbf{u}_{\bar{\theta}}(\mathbf{x}_t, t, t)\|^2]$ (the boundary gap between current parameters and the EMA copy), and the irreducible noise floor $\sigma^2 d \approx 8.2 \times 10^3$ from $\text{Tr}(\Sigma_v)$ on the same batch. table 7 reports the trajectory: the EMA-tracking proxy *decays* through training, and the shrinkage factor $\sigma^2 d / (\sigma^2 d + \|\widehat{\mathbf{b}}\|^2)$ stays near 1 throughout converged training. We caveat that $\|\widehat{\mathbf{b}}\|^2$ is the EMA-tracking gap, not the true model bias $\|\mathbf{u}_\theta(\mathbf{x}_t, t, t) - \mathbf{v}(\mathbf{x}_t, t)\|^2$; cleanly estimating the latter requires access to the conditional distribution $p(\mathbf{x}_0 | \mathbf{x}_t)$, which is intractable on ImageNet. Combined with $\kappa \approx 1$ from the Frobenius-norm Hutchinson trace, the scalar-isotropic substitution gives $\beta^* \in [0.46, 0.50]$ across the full trajectory; this is a coarse first-cut prediction that the direct matrix-form measurement (see section 5.4) refines to $\beta_{\text{no bias}}^* \approx 0.94$.

Qualitative samples. Figures 5 to 7 show 100 class-conditional generations from the three available checkpoints at step 300k, one figure per β value. The three figures share the same noise key (seed 7) and the same 100 ImageNet class labels (drawn uniformly from $\{0, \dots, 999\}$ with an independent label seed of 7, no curation), so per-position differences across the three figures isolate the effect of the loss alone. The $\beta=0$ versus $\beta=1$ contrast is at the perceptual scale, consistent with the $\sim 2\times$

Table 7: Direct DiT-checkpoint measurement of the bias-variance decomposition ingredients of Theorem 4 at $t = 0.5$. The EMA bias $\|\mathbf{b}\|^2$ averages over 128 synthetic-Gaussian \mathbf{x}_t samples and is reported for both methods. The shrinkage factor uses $\sigma^2 d \approx 8.2 \times 10^3$. The predicted β^* uses $\kappa = 1$.

| step (k) | $\ \mathbf{b}\ ^2$ (avg) | $\sigma^2 d / (\sigma^2 d + \ \mathbf{b}\ ^2)$ | β^* |
|----------|--------------------------|--|-----------|
| 20 | ~ 700 | 0.92 | 0.46 |
| 40 | ~ 150 | 0.98 | 0.49 |
| 80 | ~ 50 | 0.99 | 0.50 |

FID gap; the intermediate $\beta = 0.5$ figure is at the metric-difference scale and is not always visually separable from the baseline at this sample budget.

References

- [1] Yaron Lipman, Ricky T. Q. Chen, Heli Ben-Hamu, Maximilian Nickel, and Matt Le. Flow matching for generative modeling, 2023.
- [2] Alexander Tong, Kilian Fatras, Nikolay Malkin, Guillaume Huguette, Yanlei Zhang, Jarrid Rector-Brooks, Guy Wolf, and Yoshua Bengio. Improving and generalizing flow-based generative models with minibatch optimal transport, 2024.
- [3] Cédric Villani et al. *Optimal Transport: Old and New*, volume 338. Springer Berlin, Heidelberg, 2009.
- [4] Boris T. Polyak and Anatoli B. Juditsky. Acceleration of stochastic approximation by averaging. *SIAM Journal on Control and Optimization*, 30(4):838–855, 1992.
- [5] Antti Tarvainen and Harri Valpola. Mean teachers are better role models: Weight-averaged consistency targets improve semi-supervised learning results. In *Advances in Neural Information Processing Systems*, volume 30, 2017.
- [6] Zhengyang Geng, Yiyang Lu, Zongze Wu, Eli Shechtman, J. Zico Kolter, and Kaiming He. Improved mean flows: On the challenges of fastforward generative models, 2025.
- [7] Xinxi Zhang, Shiwei Tan, Quang Nguyen, Quan Dao, Ligong Han, Xiaoxiao He, Tunyu Zhang, Chengzhi Mao, Dimitris Metaxas, and Vladimir Pavlovic. Overcoming the curvature bottleneck in meanflow, 2026.
- [8] William Peebles and Saining Xie. Scalable diffusion models with transformers. In *Proceedings of the IEEE/CVF International Conference on Computer Vision (ICCV)*, pages 4195–4205, 2023.
- [9] Zhengyang Geng, Mingyang Deng, Xingjian Bai, J. Zico Kolter, and Kaiming He. Mean flows for one-step generative modeling, 2025.

